Numerical Methods in Civil Engineering, 10-1 (2025) 46-67

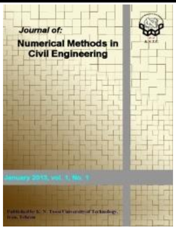

Numerical Methods in Civil Engineering

Journal Homepage: https://nmce.kntu.ac.ir/

Providing An Early Warning Protocol For Earth Dam Failures (Case Study: Shiadeh Earth Dam)

Seyed Razi Anisheh*, Mohammad Sharifipour, Arash Azari*****

ARTICLE INFO

RESEARCH PAPER

Article history:
Received:
March 2025
Revised:
October 2025
Accepted:
October 2025

Keywords:

Early Warning Protocol (EWP),
Monitoring,
Predicting settlement,
The Radial Basis Function (RBF) algorithm,
Shiadeh Earth Dam,
Instrumentation

Abstract:

Early Warning (EW) is commonly understood as the forecasting of a potentially catastrophic event. The effective use of data for EW plays a vital role in failure management, encompassing tasks like vulnerability mapping, forecasting, warning systems, prevention, planning, and the execution of actions. This study introduces an Early Warning Protocol (EWP) to tackle the potential failure of the Shiadeh Earth Dam in Iran. The dam was commissioned in 1999 and, in 2004, experienced a landslide at the downstream left abutment and the downstream slope. All installed monitoring instruments failed, meaning no deformation data has been recorded. Consequently, the Radial Basis Function (RBF) algorithm was employed to predict the dam's settlement. Satellite imagery was utilized for monitoring and controlling the dam's settlement, and a 3D PLAXIS model was used to review and evaluate the dam's performance under various reservoir conditions during different seasons, including static and dynamic states. In this study, several comprehensive phases were conducted to ensure the reliability and validity of the proposed protocol. According to the analysis results, the action plan was recognized as the central element of the EWP. Furthermore, the study highlighted that the steps of observing, planning, decision-making, and acting are essential prerequisites for the proposed protocol. By integrating satellite monitoring, numerical modeling, radial basis function algorithms, and geodetic surveying of micro-geodetic points and the dam crest alignment, this study presents an innovative and reliable protocol for monitoring the Shiadah earth dam. This approach can play a significant role in enhancing safety and reducing the risk of dam failure. Moreover, the method is applicable to all earth and concrete dams across the country. The assessment results indicate that the dam is currently at alert level 2 (caution status).

1. Introduction

Climate change is a major global challenge that affects geotechnical infrastructure and transportation systems worldwide. One area of particular concern is its impact on highway slopes and embankments (HWE). This is especially critical in regions with high rainfall and problematic soils, such as expansive clays, where changes in precipitation patterns and moisture content can have significant effects [1-6]. The increased intensity and frequency of rainfall due to climate change can weaken soil strength and increase the risk of landslides and slope failures [7]. Moreover, changes in moisture content, along with more frequent wet-dry cycles and other hydro-mechanical factors, can cause expansive clays to shrink and swell, further destabilizing highway embankments [8]. To address these challenges and account for the potential impacts of climate change on slope stability, it is essential to develop proactive strategies using effective and practical methods to ensure the long-term safety and stability of these geotechnical structures.

* PhD student, Civil Engineering Department, Razi University, Kermanshah, Iran.
** Corresponding author: Associate Professor, Department of Civil Engineering, Razi University, Kermanshah, Iran. Email: sharifipour@razi.ac.ir
*** Associate Professor, Department of Water Science and Engineering, Razi University, Kermanshah, Iran.

https://doi.org/10.61882/NMCE.2503.1084

Several studies have examined the impact of climate change on geotechnical infrastructure components [9-15]. Additionally, the interaction between soil and climate is crucial in the stability of infrastructure earthworks, particularly in relation to failure events involving highway slopes and embankments (HWEs). Climatic factors such as rainfall and temperature, in combination with highly expansive clay soils, can negatively affect embankments. Due to recent environmental changes caused by extreme events, factors such as infiltration rate, pore-water pressure, effective stress, soil suction potential, swelling and shrinkage in fine-grained soils, wet-dry cycles, vegetation cover damage, and desiccation cracks all influence the physical and hydro-mechanical behavior of soils in both the short and long term [16-19]. Wet-dry cycles can significantly impact embankment stability [20]. Excessive rainfall can lead to soil saturation, reducing soil strength and increasing susceptibility to perched water conditions and landslides.

It is noteworthy that in the 1970s, Wright conducted pioneering research on the causes of slope failures in Texas soils [21-22], addressing various factors that contribute to this issue, and his work has been widely acknowledged. Building on this foundational research, a more recent study in 2021 examined the causes of slope failures specifically in Yazoo clay (a highly expansive clay in Mississippi). This modern research focuses on the effects of rainfall and changes in groundwater levels, offering a new perspective on understanding slope instability. Moreover, expansive clay is highly plastic and sensitive to significant volume fluctuations [23]. Over 25% of the United States is covered by expansive clay soils that shrink and swell with seasonal moisture changes, making up a large portion of the land [24]. Therefore, understanding the complex relationship between soil and climate is essential for minimizing the risk of highway embankment failures and ensuring the safety and longevity of transportation infrastructure. Furthermore, regular monitoring and maintenance of embankments are vital for identifying and addressing potential instability before it becomes a serious problem, thus reducing the risk of catastrophic failures and ensuring the safety of road users. As a result, an Early Warning Protocol (EWP) could enhance the resilience of geotechnical infrastructure by providing timely and appropriate actions to reduce the likelihood of failures. The Early Warning Protocol has been defined and categorized in various ways and studied by several researchers [25-27]. Between 2004 and 2010 non-seismic HWE failures led to over 32,000 deaths globally, with many failures occurring in Asia, Central, and South America, frequently affecting low- and middle-income countries [28]. The seismic bearing capacity of shallow strip foundations on dry granular soil was investigated under inclined and eccentric loading using a modified pseudo-dynamic model. The results indicated that increased earthquake intensity and reduced soil damping significantly decrease foundation stability [29]. A model was proposed to evaluate seismic lateral earth pressures on retaining structures. The study revealed that earthquake intensity plays a significant role in increasing the pressure, and that soil-wall friction as well as foundation stiffness are key influencing factors [30]. Using the response surface method, a probabilistic evaluation of the seismic bearing capacity of shallow foundations on variable slopes was carried out. This approach reduces the need for extensive Monte Carlo simulations and facilitates reliability-based design [31]. Artificial intelligence (AI) methods for predicting shear wave velocity in soils were reviewed. The study compared different techniques, demonstrated the advantages of modern AI-based methods over traditional approaches, and identified existing research gaps [32]. The stability of reinforced slopes under seismic loading was examined. The findings showed that the reinforcement requirements depend on slope geometry, failure mechanisms, and earthquake intensity, while vertical acceleration has a relatively smaller effect [33]. It is expected that climate change, in terms of extreme events, will intensify ground instability, leading to greater human and financial losses, both direct and indirect [34]. In Figure 1, data on annual rainfall (in millimetres) at the Shiadah earth dam station since 1975 is presented. This data shows annual rainfall variations and identifies the overall trend of increasing or decreasing precipitation over the study period. Analyzing this information is highly valuable for water resource management and drought forecasting in the region.

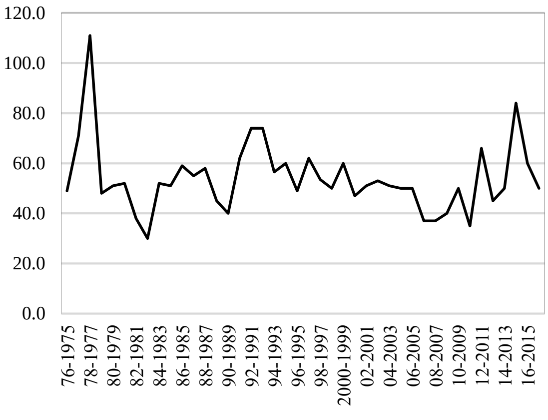

Fig. 1: Annual maximum 24-Hour rainfall statistics in millimetres

In Figure 2, the statistics of monthly average temperature (in degrees Celsius) in the dam area since 2005 are shown. This data provides useful insights into temperature trends over time and enables the analysis of seasonal changes, the impacts of climate change, and temperature fluctuations in the region.

In Figure 3, the average relative humidity (in percentage) in the study area since 2004 is displayed. This data helps analyse relative humidity patterns over time, which is crucial for understanding climate conditions, agricultural planning, and assessing the effects of humidity on the region's ecosystems [35].

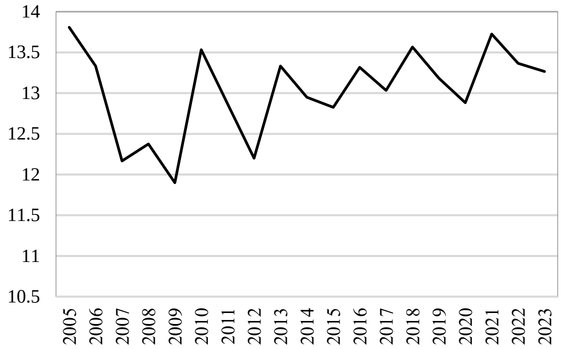

Fig. 2: Monthly average temperature statistics in degrees celsius

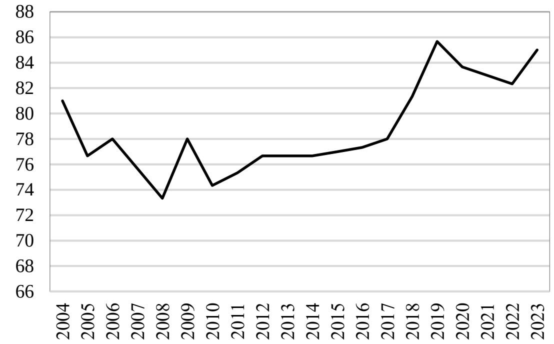

Fig. 3: Monthly average relative Statistics in percentage

The goal of this study is to develop comprehensive early warning protocols to prevent dam failures, utilizing advanced technologies, including satellite imagery. In this research, satellite images were used to analyze and calculate ground settlement and assess the risk of landslides in the downstream area of the left abutment of the Shiadeh earth dam. To enhance the accuracy of monitoring and controlling the settlement of the dam crest, three-dimensional modeling was carried out using PLAXIS 3D software. The results of this modeling showed a strong correlation with ground survey data and were particularly effective in predicting settlement on the downstream slope using the RBF algorithm. These findings confirm the effectiveness of this method for precise monitoring and predicting potential dam issues. This study can serve as a model for designing and implementing early warning protocols for similar dams and play a crucial role in reducing risks and improving dam safety.

This study also proposes a slope vulnerability index based on an Early Warning Protocol (EWP) for the external slopes and settlement of the Shiadeh earth dam crest. The following steps were undertaken to develop this protocol; a) Conducting field investigations and selecting the complete study area b) Collecting results from geotechnical tests in the study area c) Gathering data from installed instrumentation up to 2013, which were verified to be functional and accurate d) Conducting micro-geodetic surveys of the dam's external slope and preparing a longitudinal profile along the dam crest e) Predicting settlement using advanced RBF algorithms f) Analyzing the dam foundation and body using PLAXIS 3D software to calculate settlement and deformation g) Using satellite imagery to calculate settlement in the dam area h) Performing parametric studies on various factors and developing an early warning protocol for slope and crest failures.

2. METHODOLOGY

In this study, four main steps were considered for monitoring settlement and assessing the dam's condition:

1. Field Investigations:

This step included site surveys and ground mapping of micro-geodetic points on the downstream slope and the dam crest. The goal was to gather precise data for modeling movements and deformations at different locations of the dam to better analyze its stability. The present study was conducted within the area of a specific earth dam located in Mazandaran Province. The dam benefits from recorded settlement gauge data collected between 1999 and 2012 (1378 to 1391 in the Iranian calendar) by instruments installed on the downstream slope, reliable geotechnical results, and access to terrestrial surveying data conducted in 1999 and 2013 (1378 and 1392).

2. Settlement Prediction:

In this stage, the RBF (Radial Basis Function) algorithm was used to predict settlement based on data from installed instruments on the downstream slope of the dam. The instruments were in proper working condition, and a total of 530 data points were recorded and measured. These data were specifically utilized for analyzing the behavior and predicting settlement changes of the dam.

RBF approximation method based on Lagrange multipliers was presented by Fasshauer in Chapter 19. This section provides a summary of its main characteristics. In this method, the problem is formulated as a constrained quadratic optimization, aiming to find an appropriate function to approximate the given dataset. The function is adjusted using Lagrange multipliers to achieve the best possible fit to the data and ensure high accuracy in approximation :

$$f(X) = \sum_{j=1}^{M} R_j \beta(\|X - \Upsilon_J\| \qquad (1)$$

In this approach, the function $f(X)$ is constructed as a weighted sum of radial basis functions M (RBFs), each linked to a specific reference point Υ_J, and assigned a coefficient R_j. The goal is to determine the weight R=($R_1 . \dots \dots . R_N)^W$ vector by minimizing the quadratic form:

$$f(X) = R^W \mathrm{QR} \quad (2)$$

Where Q is an M × M symmetric positive definite matrix. This minimization is subject to linear constraints SR=t, where S is a full-rank N × M matrix, and $t=(t_1.\dots\dots.t_N)^W$ is a given vector. This optimization problem can be reformulated as a least-squares estimation (LSE):

$$f(R.U) = \frac{1}{2} R^W \mathrm{QR}\text{-} U^W (SR - t) \quad (3)$$

Here, $U=(U_1.\dots\dots.U_N)^W$ represents the Lagrange multipliers, and the objective is to minimize (3) with respect to R both and U . This leads to solving the following system:

$$\frac{\partial F(R.U)}{\partial R} = QR - S^W U = 0$$
$$\frac{\partial F(R.U)}{\partial U} = SR - t = 0 \quad (4)$$

which, in matrix notation, takes the form:

$$\begin{pmatrix} Q & -S^W \\ S & 0 \end{pmatrix}\begin{pmatrix} R \\ U \end{pmatrix} = \begin{pmatrix} 0 \\ t \end{pmatrix} \quad (5)$$

Where $Q_{i.j}=\beta(\|\Upsilon_i - \Upsilon_j\|)$, and Q is symmetric. The solution to Equation (5) provides the final weights. To enhance computational efficiency, it is beneficial to minimize M, thereby reducing the cost of evaluating the approximated value $f(X)$ [36].

3. Static and Dynamic Analyses:
Static and dynamic analyses of the earth dam were performed using the 3D Plaxis software. The analyses considered the lateral supports and the interaction between the foundation, dam body, and reservoir.

All conditions of the reservoir filling at various levels were evaluated throughout all seasons to accurately assess the effects of static and dynamic loads on the dam's stability.
These steps were designed to thoroughly assess the dam's condition and predict settlement changes. They not only provide detailed analysis of the dam’s status but also enable timely decision-making to prevent potential issues in the future.

4. Employing satellite imagery to calculate dam settlement. The data used in this research corresponds to a specific time period, during which both instrumentation data and Sentinel-1 satellite imagery (from 2014 to 2024) were available. Since the Sentinel-1 satellite was launched in 2014, it is not possible to obtain satellite images from before that year.
This study does not cover topics such as hydraulic analysis of the dam, spillway performance, or project economics.

3. Interferogram Generation and Coregistration

Two split-orbit SAR images were coregistered using a back-geocoding operator to match the slave image with the master image, creating a single-master stack. This process involved using an external DEM (SRTM 3Sec HGT) for reference. The back-geocoding operator also corrected geometric distortions in the SAR images. A small data block in the burst center was used to calculate a fixed range offset, and an ESD approach estimated a fixed azimuth portion. An interferogram was created, considering terrain displacement, acquisition geometry, and atmospheric conditions. The total interferometric phase includes contributions from displacement, topography, flat earth, and atmosphere. The overlapping black line in each burst was removed using TOPSAR Deburst, ensuring continuous coverage of burst data [37]. SAR images are represented by square pixels, with each pixel's amplitude and phase values used to create a two-dimensional complex image. After registration, the complex SAR images were multiplied, and the interferometric phase was extracted using Equation 6.

$$S = Be^{-j\Phi} = Be^{-j\frac{4\pi}{\gamma}d} \quad (6)$$

In this context, S represents the measured complex signal of a SAR image, B is the amplitude, $j\Phi$ is the recorded phase, and d is the distance in the slant range direction between the sensor and a particular scatterer [38]. Let S1 and S2 denote the received signals from two satellite positions. The first image (S1) is referred to as the master image (pre-event), and the second image (S2) is referred to as the slave image (post-event). Consequently, S1 and S2 are expressed by Equations (7) and (8). After registration, the two complex SAR images are multiplied, and the interferometric phase is derived using Equation (9).

$$S_1 = B_1 e^{-j\Phi} = B_1 e^{-j\frac{4\pi}{\gamma}d_1}, \quad (7)$$

$$S_2 = B_2 e^{-j\Phi} = B_2 e^{-j\frac{4\pi}{\gamma}d_2} \quad (8)$$

$$S_1 S_2 = B_1 B_2 e^{-j\Phi} = B_1 B_2 e^{-j\frac{4\pi}{\gamma}(d_1 - d_2)} \quad (9)$$

3.1 Phase Unwrapping, and Displacement Mapping

Differential SAR Interferometry (DInSAR) is a technique used to measure Earth surface displacements with centimeter-level accuracy. The interferometric phase is calculated using Eq. (10). The SRTM 3Sec HGT auto-download DEM is used to remove topographic phase contributions and create an interferogram showing only displacement. The Multi-look driver eliminates spectral noise, improving image resolution. A Goldstein filtering operator is applied to reduce phase noise. SNAPHU software performs 2-D phase unwrapping using the Minimum Cost Flow (MCF) method. SNAPHU, a Linux-based tool, requires command line programming and is not part of the SNAP software. After processing, the unwrapped phase is imported into SNAP, where it is converted into deformation data.
At least two satellite constellation images are required to generate an interferogram, which includes topographic components, atmospheric effects, baseline error, and noise [39-40].

$$\Psi=\Psi_{disp}+\Psi_{flat}+\Psi_{topo}+\Psi_{atm}+\Psi_{orbit}+\Psi_{noise} \quad (10)$$

Where Ψdisp represents the line-of-sight (LOS) displacement, Ψflat the flat Earth phase, Ψtopo the topographic phase, Ψatm the atmospheric phase, Ψorbit the baseline error phase, and Ψnoise the noise phase contribution [41]. In satellite imagery, there are some limitations related to atmospheric noise and vegetation.

Atmospheric Noise in Sentinel-1: Atmospheric noise such as clouds and fog has almost no effect on Sentinel-1 images because the satellite uses microwave radar that penetrates clouds. Only heavy precipitation may slightly weaken the signal. The main noise in these images is speckle noise caused by radar wave scattering on the target surface, unrelated to atmospheric conditions.

Vegetation in Sentinel-1: Dense vegetation produces strong radar reflections, but accurately distinguishing plant types or density is challenging. Leaves and stems cause complex wave scattering, and in sparse vegetation, signals from soil and plants mix, making interpretation difficult.

3.2 InSAR Terrain Correction

To correct for terrain-induced errors in satellite tilt and backscatter readings, a Range Doppler Terrain correction was applied. By using reference DEM data and an external precise orbit, specific geolocation information is obtained to remove these distortions. This correction is applied to the differential interferogram, displacement map, and coherence to prepare them for export and viewing on Google Earth.

In this study, to effectively implement the developed Early Warning Protocol (EWP), four main steps were considered; employing satellite imagery to calculate dam settlement in relation to existing faults in the vicinity, performing field investigations including micro-geodetic surveys of the downstream slope and the dam crest, predicting settlement using instrumentation when it was in proper working condition, conducting static and dynamic analyses of the earth dam using 3D Plaxis software for all reservoir filling conditions, and It should be noted that implementing all the proposed steps is not mandatory for applying this protocol. Due to its height of over 30 meters, the Shiadeh Dam is classified as a large dam according to the guidelines of the International Commission on Large Dams (ICOLD). One of the key criteria for assessing dam safety is the stability of slopes. In this study, 13 phases of 3D modeling using PLAXIS software were conducted, all of which demonstrated acceptable safety factors. These results are in full compliance with the standards outlined in the "Guidelines for Seismic Analysis and Design of Earth and Rockfill Dams" (Publication No. 624). Therefore, it can be concluded that the modeling provides a reliable assessment of the Shiadeh Dam's stability. For slopes with fewer initial signs of movement or deformation, fewer monitoring tools, limited field and laboratory tests, and a simplified numerical analysis may be sufficient to achieve the desired predictive outcomes.

4. SITE SELECTION (INVENTORY)

The Shiadeh earth dam, located 35 kilometers southwest of Babol city in Mazandaran Province, has been studied at the UTM coordinates x = 636028 and y = 4021865.The Shiadeh earth dam is located 35 kilometers southwest of Babol city in Mazandaran Province. According to ICOLD classification, the Shiadeh rockfill dam with a clay core is categorized as a high dam and is considered a significant structure. The dam's crest length is 450 meters, and its height from the riverbed is 33.0 meters. The dam was constructed in 1999 to supply irrigation water for downstream agricultural lands. Figure 4 illustrates the area of a landslide that occurred in 2004 at the downstream left abutment and the toe of the earth dam.

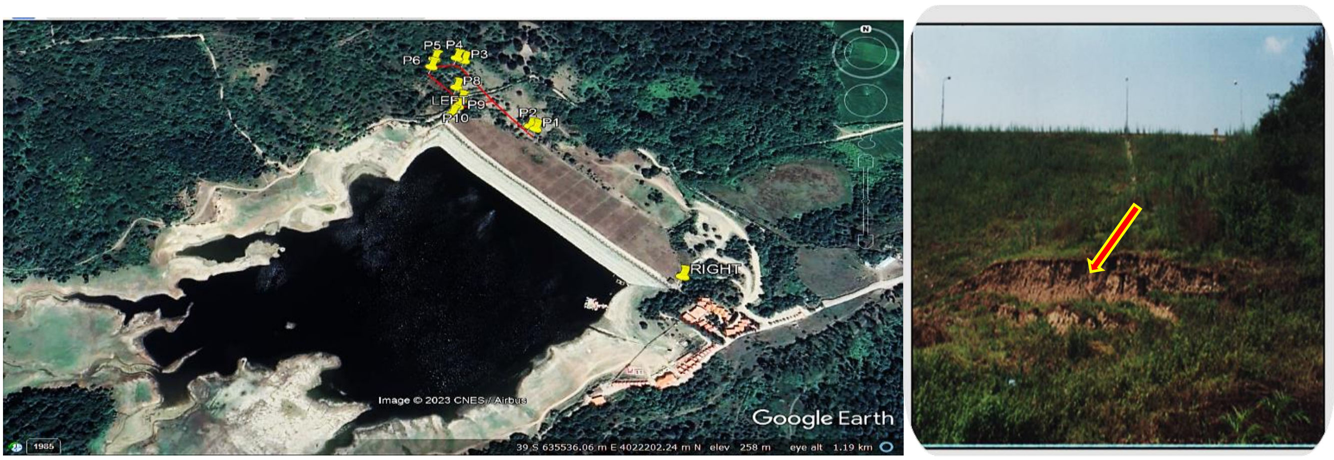

Fig. 4: Landslide downstream of the left abutment and shallow sliding at the dam toe

Figure 5, from the geological map of Iran (Qaemshahr Sheet), shows that the dam site is located on Pliocene-aged formations. These formations consist of alternating layers of conglomerate, marl with silt, sandstone, and siltstone. The geological features indicate that the dam site is situated in a structurally complex area with the potential for active tectonic influences due to the proximity of active faults. Careful geotechnical investigations and fault activity assessments are necessary to ensure the stability and safety of the dam structure.

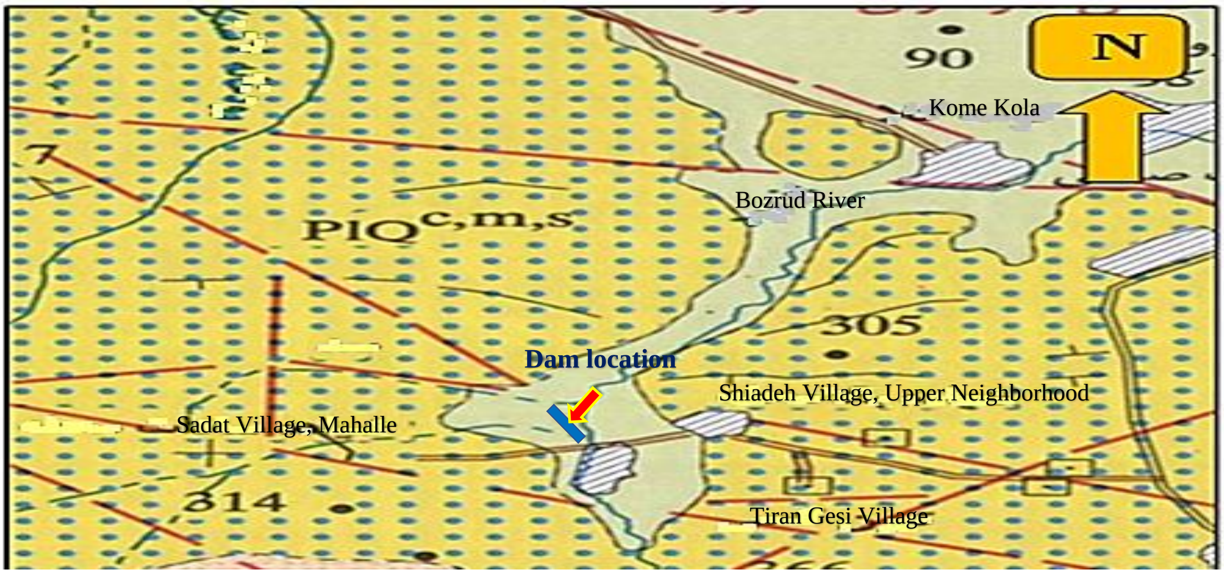

Fig. 5: The geological map of the Shiadeh Dams

The figure 6 depicts the mountain-plain fault, the Shiadeh fault, and the Kelaroud fault. This slide served as a warning of potential triggering factors that could threaten the dam in the future. The depth of the faults ranges from 6 to 22 kilometers and they are classified as thrust or reverse faults. These types of faults are formed due to compressive stresses, causing the Earth's layers to move upward and overlap. Such faults typically develop in regions with compressive tectonic stresses, such as mountainous areas or at the boundaries of converging plates. These faults can lead to strong earthquakes and significant alterations in the Earth's structure.

One of the reasons the Shiadeh and Kelaroud faults are of interest is that they receive energy from ancient or primary faults and can cause slips within the site area. These slips may increase geotechnical hazards and have potential impacts on the stability of structures and infrastructure in nearby regions. Therefore, a thorough investigation of secondary faults and their influence is essential in seismic hazard analysis.

The secondary fault identified at the left abutment of the dam site is evidenced by various geological signs, including irregular stratification, landslides at the left abutment, and the dam toe since the beginning of operation. These observations indicate that the fault is either active or has been reactivated due to the reservoir's saturated environment, leading to settlement and landslides at the left abutment. One of the confirming factors for the presence of this secondary fault is the existence of a natural spring downstream of the Shiadeh dam, which suggests groundwater flow associated with fault activity.

Therefore, in this study, settlement and triggering factors, such as the faults in the construction site's vicinity, were investigated using Sentinel-1 satellite imagery. As part of the Copernicus initiative by the European Space Agency (ESA), free satellite data and information services are available through the Data and Information Access Services (DIAS) or the Conventional Data Hub (Copernicus Open Access Hub) [42]. The Copernicus Open Access Hub grants access to Sentinel data for all users, especially those within the European Union. Before access can be granted, the user registration process must be completed. This platform allows users to obtain satellite imagery and download preprocessing software in various versions. In this study, version 7.0 of SNAP was utilized for preprocessing. The IW Mode (Interferometric Wide Swath Mode) is one of the imaging modes of Sentinel-1 satellites under the Copernicus program. This mode is specifically designed for applications such as mapping ground changes and radar interferometry analysis (InSAR). One of the key features of the IW Mode is its ability to cover a wide area of approximately 250 kilometers in each satellite pass. The IW Mode has a spatial resolution of approximately 5 × 20 meters (in range and azimuth directions). It supports various polarizations, including VV, VH, HH, HV, which can be adjusted depending on the application. In this project, the VV polarization was used to calculate the settlement of the dam and its surrounding area.

Figure 7 illustrates the settings for downloading Sentinel-1 satellite imagery. A square region with dimensions of 26.9 × 26.9 km and a total area of 724 square kilometers has been defined to encompass the dam. The polarization settings are configured to VV, which is highly suitable and accurate for analyzing dam settlement, supporting structures, and even minor existing faults. The availability of VV-polarized images since then has enabled consistent monitoring and analysis of the study area. The satellite image data analyzed inthis study are presented in Table 1.

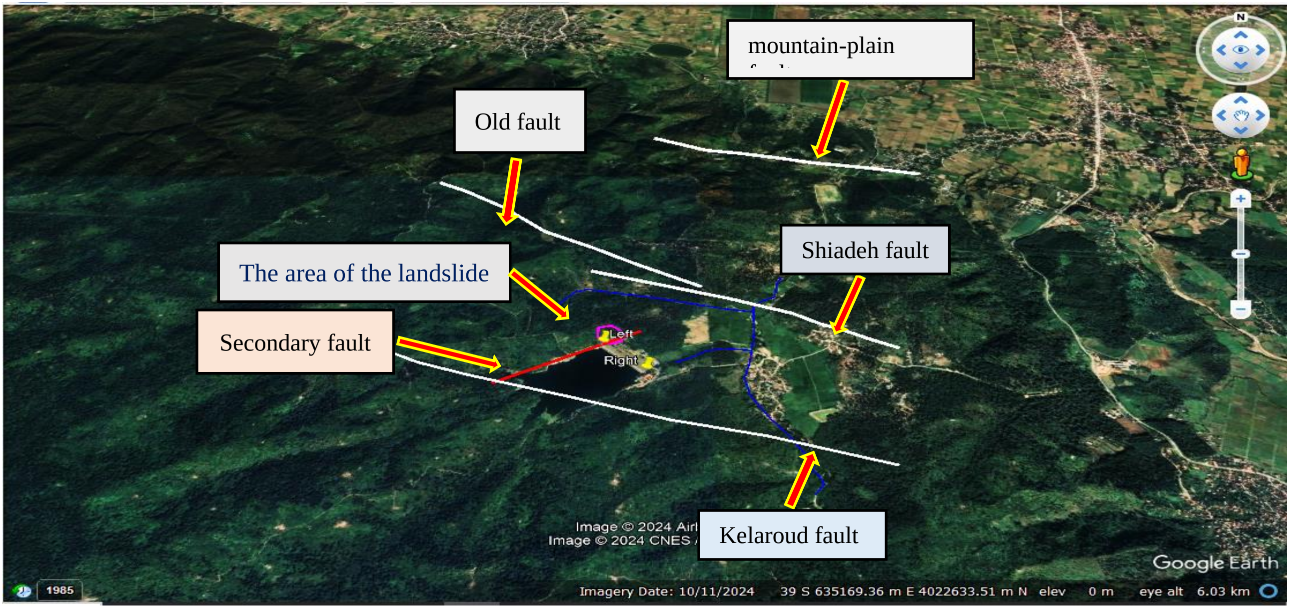

Fig. 6: Location of Shiadeh Earthen dam site

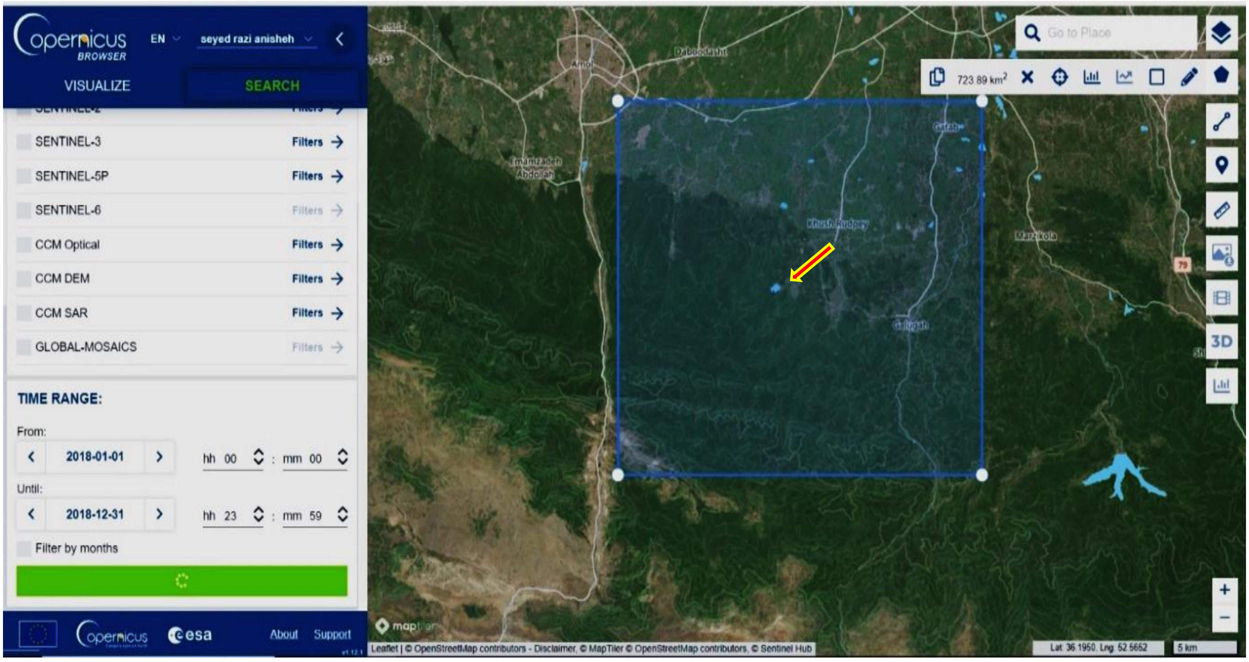

Fig. 7: Illustrates the settings for downloading Sentinel-1 satellite imagery

Table 1: Summary of satellite image data and specofications

Temporal coverage	Mission	Product type	Acquisition mode	Pass direction	polarization
S1A-IW-SLC-2014-12-25	sentinel-1	SLC	IW	Ascending	VV
S1A-IW-SLC-2015-11-28	sentinel-1	SLC	IW	Ascending	VV
S1A-IW-SLC-2016-7-23	sentinel-1	SLC	IW	Ascending	VV
S1A-IW-SLC-2024-01-07	sentinel-1	SLC	IW	Ascending	VV

5. SAR PRE- PROCESSING STEPS

In the Topsar-Split system, there are three types of swaths: IW1, IW2, and IW3. When the satellite captures an image in ascending mode (from the North Pole to the South Pole), the order of the swaths in the satellite image is as follows: IW1 is on the left side of the image, IW2 is in the middle, and IW3 is on the right side of the image. Each satellite image consists of 9 horizontal sections, referred to as bursts. The lowest horizontal section (burst 1) is at the bottom of the image, and the highest horizontal section (burst 9) is at the top.

By knowing the location of the study project, the order of the IW swaths and bursts can be adjusted to speed up the analysis process in the SNAP software.

VV polarization means that both the transmission and reception polarization are vertical.

In interferometry and for calculating the amount of subsidence and settlement in this study, VV polarization has been used. Before starting the processing, the images need to be checked for coherence. A window will open, and by clicking the "Add opened" button, the names of the two IW satellite images in SLC format will appear. One of the images is designated as the Master, and the other as the Slave. Another important specification is that the Track number of both images must be the same, which in this study is 130. To assess the suitability of the images, Modeled coherence is used. If the Modeled coherence value falls between 0.6 and 1, then the images are considered suitable for processing [43].

5.1 SAR PROCESSING STEPS

Sentinel-1 SAR data was processed using the open-source Sentinel Applications Platform (SNAP) software, version 7.0 (ESA,2014). Within the SNAP environment, the Sentinel-1 Toolbox was used to perform the processing steps step-by-step, as illustrated in Figure 8.

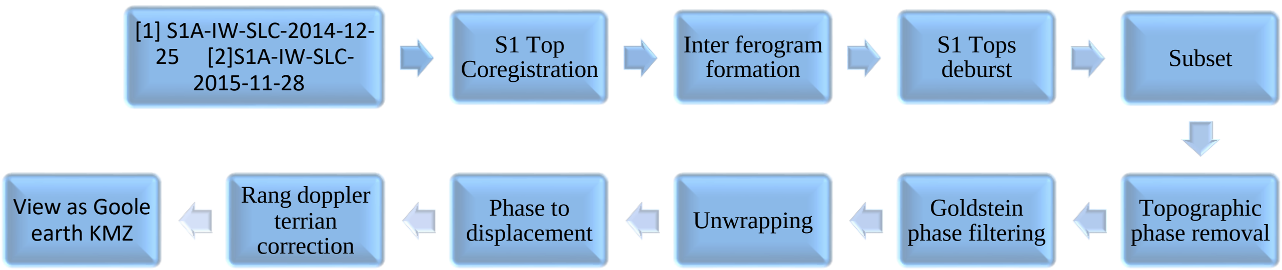

Fig. 8: step-by-step satellite image processing

6. SIMULATION

In the processing using SNAP software, during the Unwrapping phase, the results are displayed in a color spectrum format. It is worth mentioning that the Sentinel-1A satellite was launched on April 3, 2014, and Sentinel-1B on April 25, 2016. Therefore, the earliest Sentinel-1 satellite images available for download date back to 2014. Access to VV polarization images since then has enabled accurate monitoring and analysis of the study area. However, due to limited temporal coverage, the use of images prior to 2014 was not possible in this.

To continue the analysis and extract vertical deformation or land subsidence across all areas covered by the satellite images, it is essential to perform the "Phase to Displacement" processing step. This step is a key component of the radar interferometric process and is illustrated as an example in Figure 8. One of the important steps in this process is converting the phase data obtained from interferometric processing into actual displacement values.

The images used in this processing, corresponding to different years of the study period, are presented separately in Figures 9, 10, and 11. On the left side of these images, a red box highlights a wide area of the dam site that is affected by all existing faults, ground movements, and other natural effects in the study area. The results of this analysis include the cumulative vertical deformation or subsidence, which is well represented by a color spectrum showing the variations. It is worth noting that at this preprocessing stage, assigning UTM coordinates to the dam site is not possible.

To monitor the condition of the dam and its surroundings, special satellite images were used that can show even the smallest changes in the ground surface. This method requires no installation of any devices on the ground and can detect very slight changes (for example, on the order of a few centimeters). Using these images is both inexpensive and allows for regular monitoring over a wide area. With this information, deformation or settlement of the dam over different time periods can be determined.

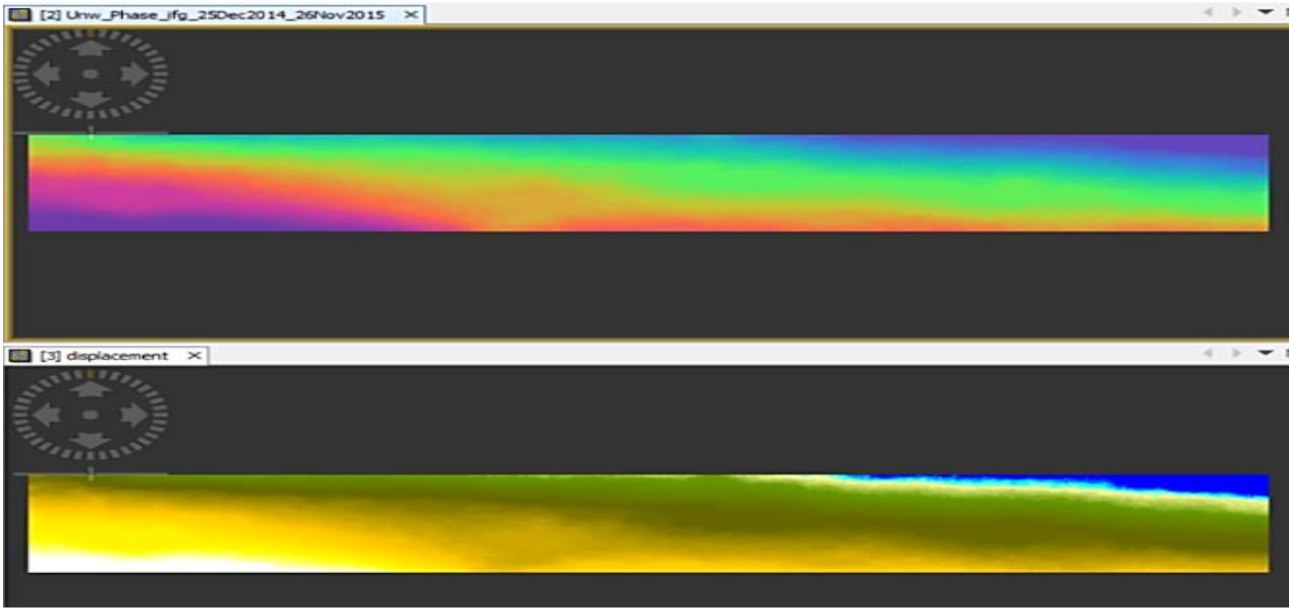

Fig. 9: Vertical displacement related to the images from the years 2014 and 2015

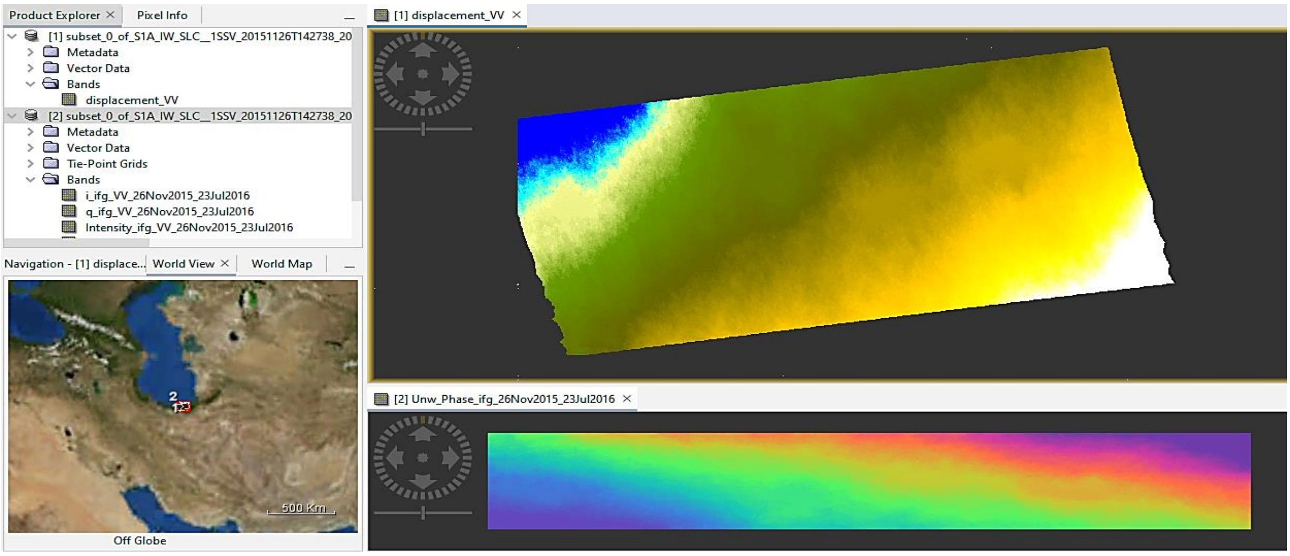

Fig. 10: Vertical displacement related to the images from the years 2015 and 2016

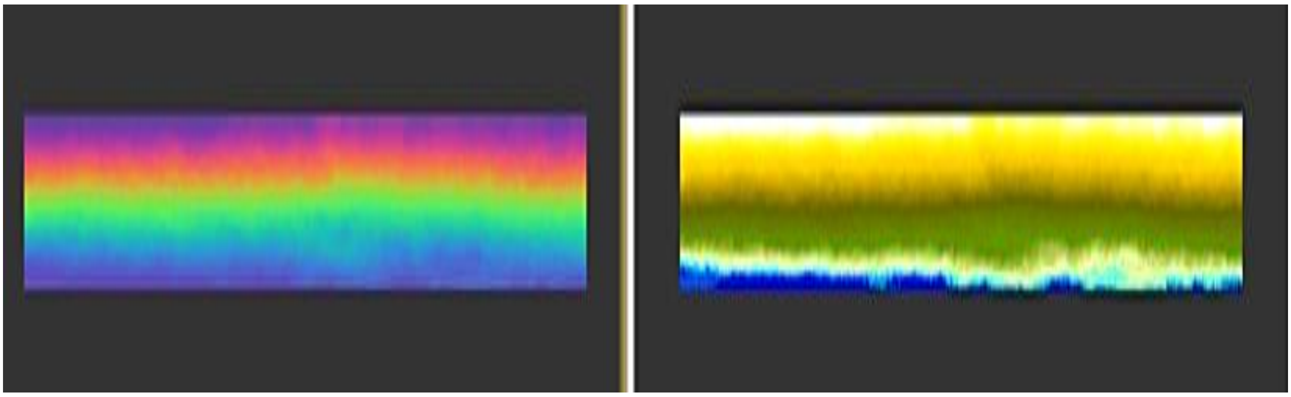

Fig. 11: Vertical displacement related to the images from the years 2016 and 2024

In Figure 12, the final results of processing Sentinel-1A satellite images with IDs S1A-IW-SLC-2014-12-2 and S1A-IW-SLC-2015-11-28 using SNAP software are presented as a vertical displacement (subsidence) map. These results are imported into Google Earth software to accurately display the geographic coordinates of all structural components under study, while also visualizing the amount of vertical ground deformation or subsidence through a color spectrum in metric units. According to the map legend, the maximum subsidence observed at the dam crest reaches approximately -0.05 meters (equivalent to 5 centimeters).

This amount of subsidence reflects the combined influence of all faults present in the study area, each with distinct geological characteristics, and also includes the effects of seismic activity that may have occurred during the operational phase of the dam. In this figure, the main faults of the region—including the mountain-front faults, the active Shiadeh fault, and the old Kelaroud fault—are marked with white lines, while secondary faults are indicated with red lines. This graphical representation enables a more detailed analysis of the tectonic structures' role in vertical ground deformation.

For the processing of the satellite images S1A-IW-SLC-2015-11-28 and S1A-IW-SLC-2016-07-23 in SNAP software, the same processing steps used in previous analyses were followed again. The results of this processing are presented in Figure 13 as a color-coded displacement map, illustrating the amount of vertical displacement or ground subsidence along the dam crest. According to the color legend on the left side of the map, the subsidence during this period is estimated at approximately -0.02 meters (equivalent to 2 centimeters).

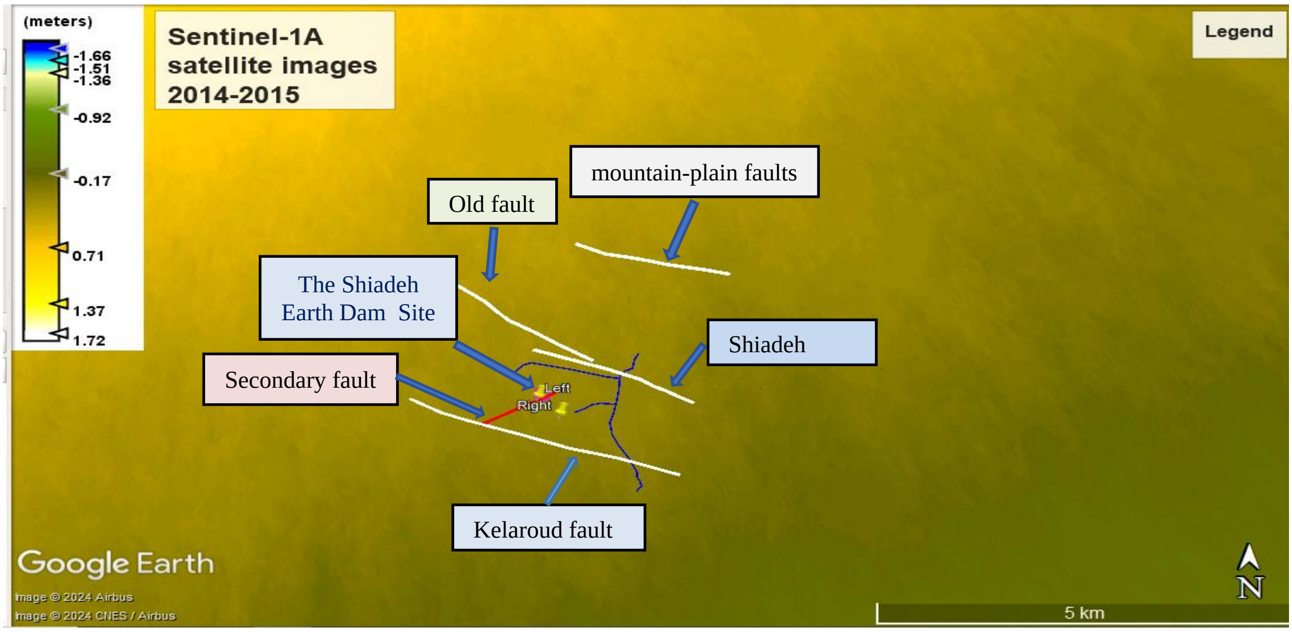

Fig. 12: Faults are represented by white lines, with vertical displacement at the left and right dam abutments shown using a color scale.

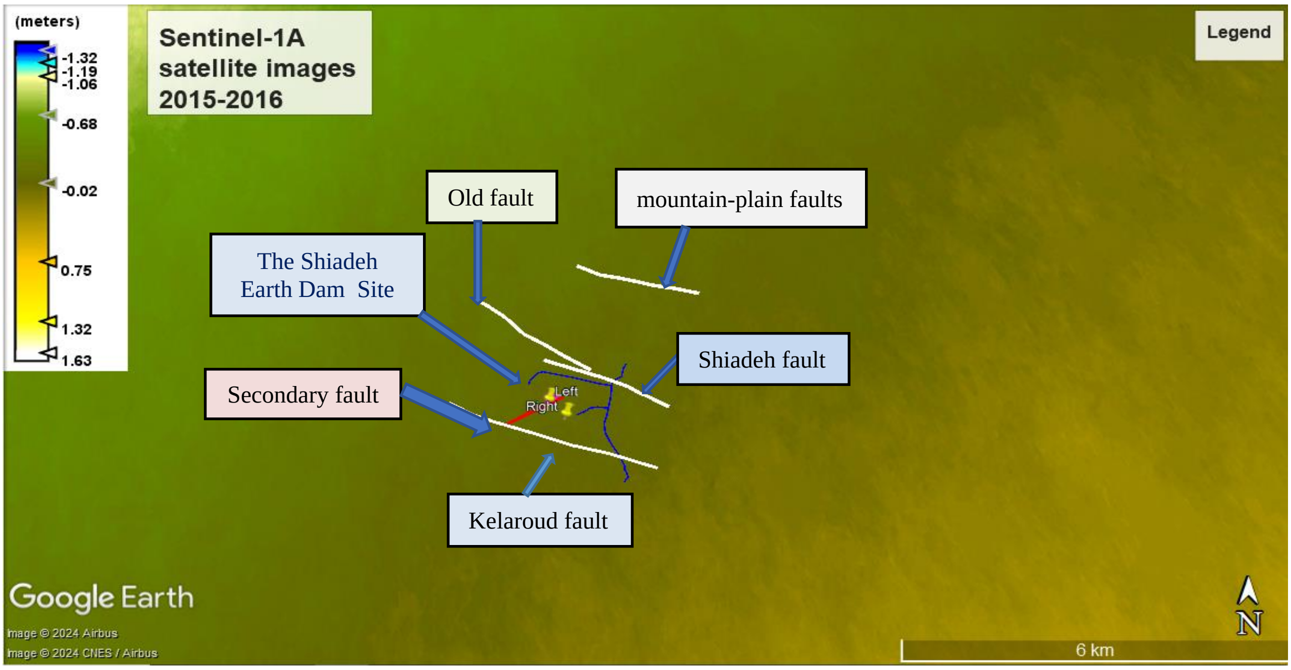

Fig. 13: Faults are depicted with white lines, and vertical displacement at the left and right dam abutments is visualized with a color scale

Similarly, for the processing of satellite images S1A-IW-SLC-2016-07-23 and S1A-IW-SLC-2024-01-07, the same processing approach in SNAP software was applied. The results of this stage are shown in Figure 14, which illustrates vertical subsidence using a color spectrum in metric units. Based on the color scale on the left side of the image, the amount of subsidence during this period is approximately -0.80 meters (equivalent to 80 centimeters). By zooming in on Figure 14, the color variations representing vertical displacement can be clearly observed in the left and right abutments of the Shiadeh Dam, highlighting areas of significant deformation.

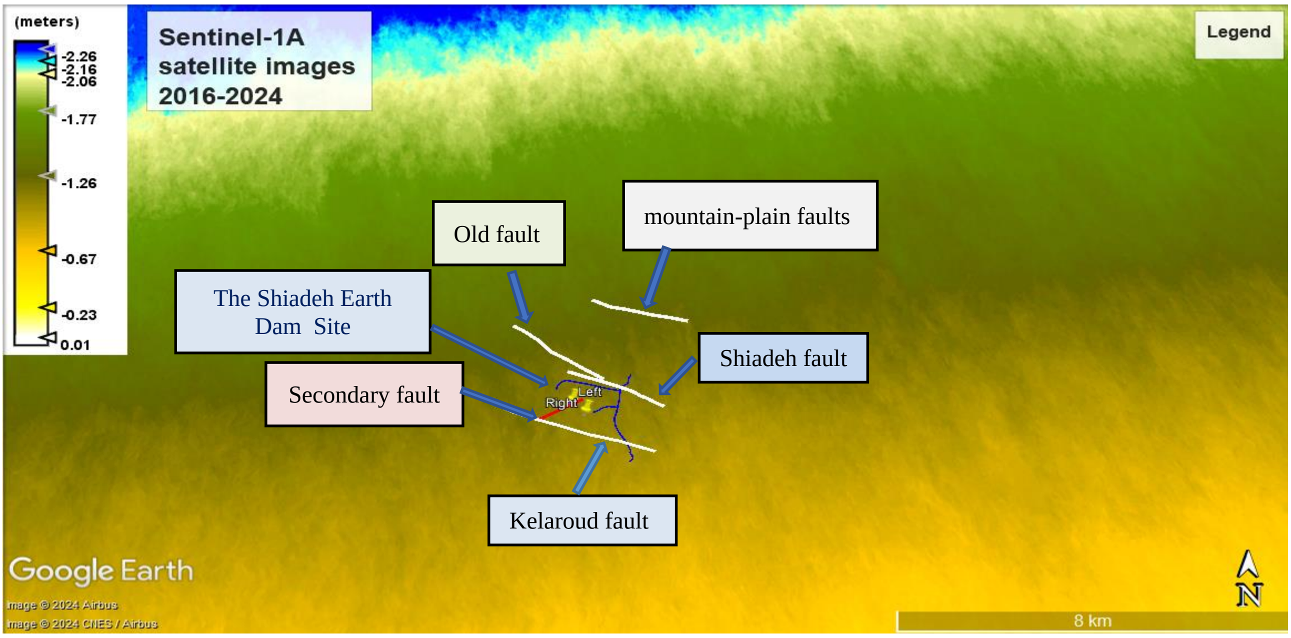

Fig. 14: The faults are shown with white lines, and the vertical displacement at the left and right abutments of the dam is represented using the color scale.

In the preprocessing stage of satellite imagery, ground surface changes were used as the basis for analysis, and the calculation accuracy reached centimeter-level precision. In Figures 12, 13, and 14, all points within the extensive area of the dam site are presented using UTM coordinates and displayed in a color spectrum. By referring to the color legend shown on the left side of the maps, the amount of ground settlement at each point can be clearly interpreted.The total cumulative settlement along the crest of the Shiadeh earth dam was calculated to be 87 centimeters using time-series analysis of radar satellite images over the period from 2014 to 2024. This amount of settlement was obtained using the Interferometric Synthetic Aperture Radar (InSAR) technique without the need to install any ground-based equipment. Following the completion of dam construction in 1999, a ground survey was conducted in 2012 along the dam crest (as shown in Figure 15). The dam was commissioned in 1999. After several years, in 2012, a monitoring campaign was conducted to assess settlement along the dam crest. The results, presented in Figure 15, revealed non-uniform settlement across the crest. However, no systematic monitoring was carried out by the operating team during this period to accurately track or analyze the settlement behavior. This significant settlement is most likely attributed to the influence of geological faults located near the left abutment of the dam site. Subsequently, a second phase of ground surveying was carried out in 2024. However, the data obtained from this phase were not used as a comparative reference, as between the two surveys, the Mazandaran Regional Water Company had carried out gravel filling, leveling, and repair works along various sections of the earth dam crest. These interventions altered the surface conditions of the crest, making a direct comparison between the 2024 data and the 2012 results invalid [44].

Land surveying during the period from 1999 to 2012 was carried out using dual-frequency GPS systems and total station instruments. This operation was conducted based on existing and well-established benchmark points to ensure measurement accuracy at the millimeter level. The use of dual-frequency GPS enabled the correction of atmospheric and ionospheric errors, guaranteeing very high positional accuracy. Additionally, total stations, with their precise angular and distance measurement capabilities, provided highly sensitive coordinate acquisition. This combination of technologies resulted in high-quality and reliable land surveying data.

Figure 16 illustrates the layout of micro geodetic points installed along seven axes on the downstream slope of the Shiadeh earth dam.

Figure 17 illustrates a comparison of the positions of micro-geodetic points on the downstream slope of the dam, obtained through high-precision ground-based surveying with millimeter-level accuracy. In this figure, the horizontal axis represents the distance from the edge of the dam crest toward the downstream slope, while the vertical axis shows the local elevation codes of various points along the dam body. The results clearly indicate the occurrence of uplift or swelling in the downstream slope of the dam over the period from 1999 to 2024. The swelling has been measured to be at least between 20 centimeters and 40 centimeters.

7. THE PROPOSED RADIAL BASIS FUNCTION (RBF)

In Table 2, the elevation code of the instrumentation for the installation on the downstream slope of the Shiadeh earth dam is shown for settlement measurement.

During the years when the instrumentation was functioning properly, a total of 530 data entries related to settlement were recorded, which served as the basis for settlement prediction calculations using the RBF algorithm [45].

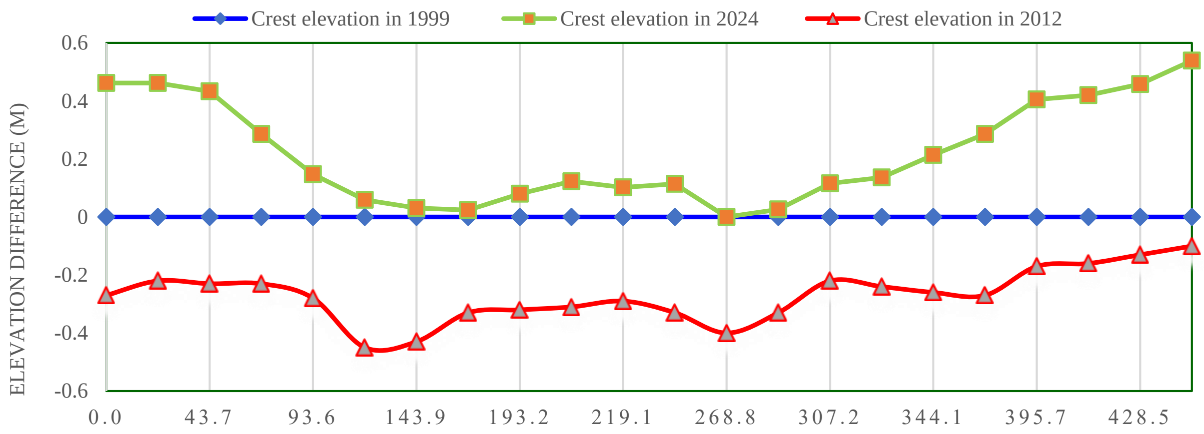

Fig. 15: Comparison of Ground survey from 1999 with 2012

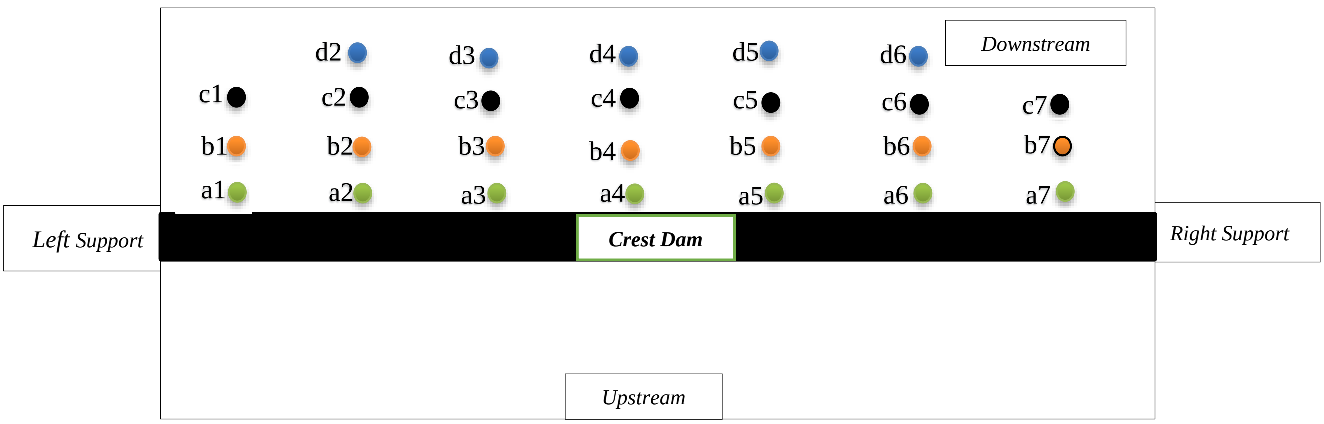

Fig. 16: Placement of micro-geodetic points on the downstream slope of the Shiadeh earth dam

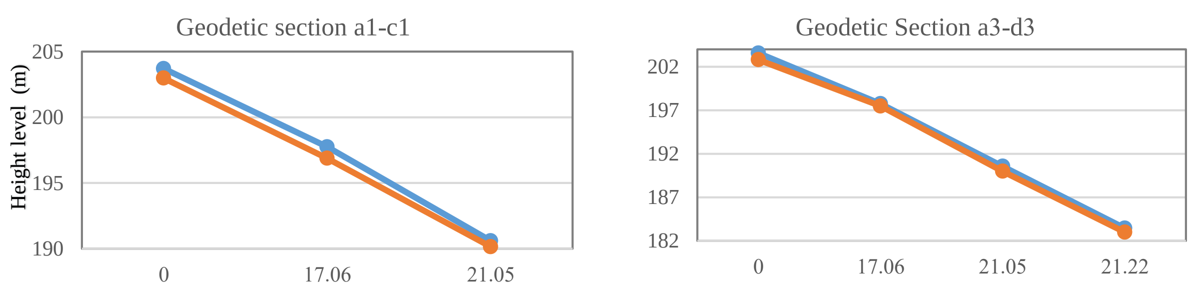

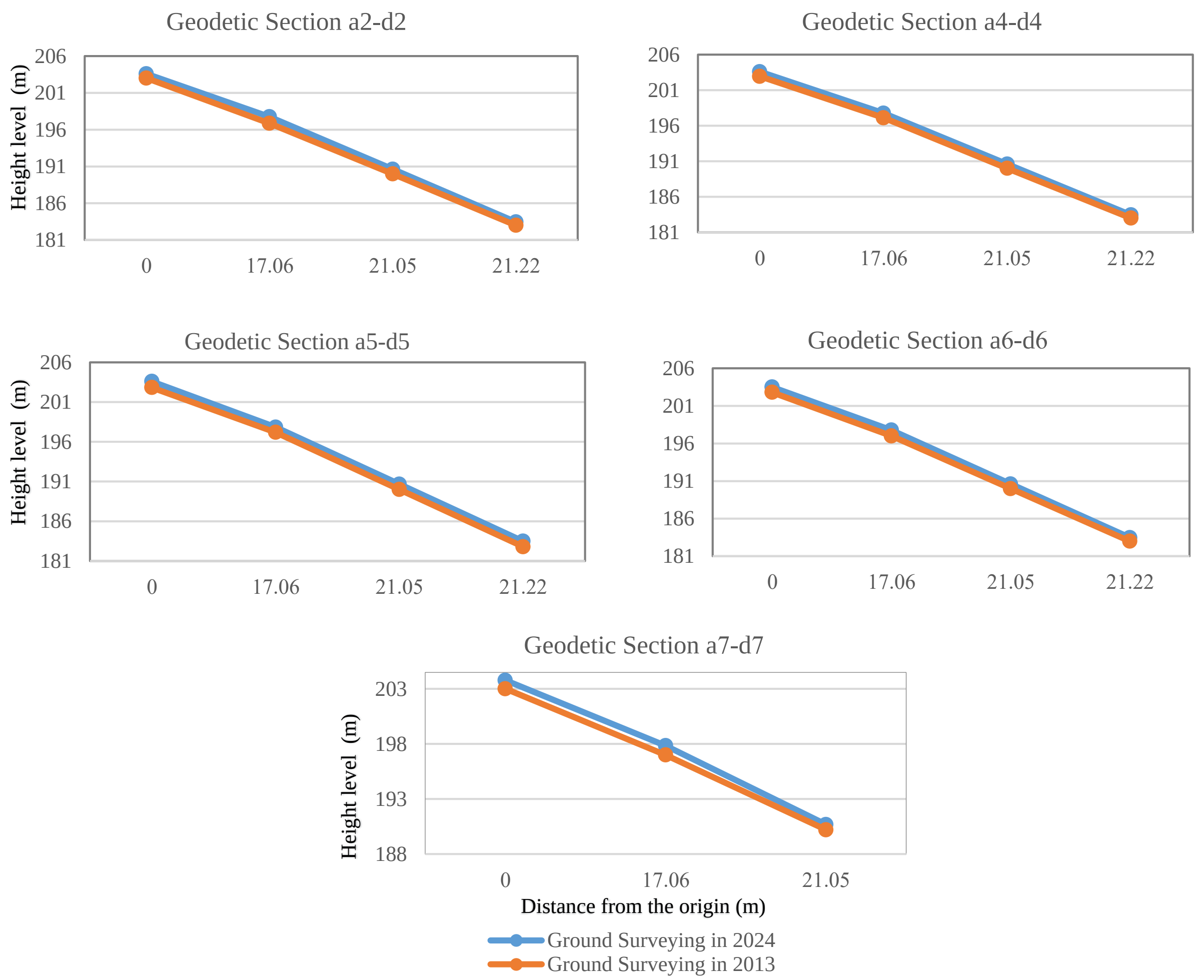

Fig. 17: Several cross-sections of the micro geodetic points, clearly demonstrating the swelling or uplift of the downstream slope of the earth dam

Table. 2: The elevation code of the instrumentation

Precision tools axis A	Install level	Precision tools axis B	Install level	Precision tools axis C	Install level
A1	179.6	B1	178	C1	176.25
A2	180.11	B2	178.51	C2	178.9
A3	182.75	B3	181.27	C3	182.51
A4	186.42	B4	185.07	C4	186.19
A5	190.19	B5	188.83	C5	189.84
A6	193.98	B6	196.38	C6	-

The layout plan of the piezometers, observation wells, and other geotechnical instruments—including inclinometers and settlement gauges—on the downstream slope of the Shiadeh earth dam is illustrated in Figure 18 using solid circles along three cross-sections: A, B, and C. These instruments have been continuously monitored and recorded since the commencement of the dam's operation. The collected data has been systematically measured and documented over time. Furthermore, the accuracy and functionality of these instruments have been confirmed by the dam operation unit under the supervision of the Mazandaran Regional Water Authority. All installed instruments operated flawlessly and were fully functional from the start of the dam's operation on August 9, 1999, until October 10, 2012. However, after 2012, all the installed instruments ceased to function, leaving only three operational piezometers.

The main cause of the piezometer failures was the bending and deformation of the piezometer tube during the dam's operational period, which prevented

the measuring sensor inside the piezometer borehole from moving freely. Consequently, accurate measurement of the water level was not possible. This issue disrupted the continuous and precise monitoring of pore water pressure within the dam. To resolve this problem and continue the monitoring process, the Mazandaran Regional Water Company has drilled observation wells on the left bank of the dam site. Through these wells, changes in the water level can be measured directly and reliably, enabling effective monitoring of the dam's hydraulic Therefore, to monitor the dam, several observation wells were designed on the downstream slope and left abutment, and included in the execution plan.

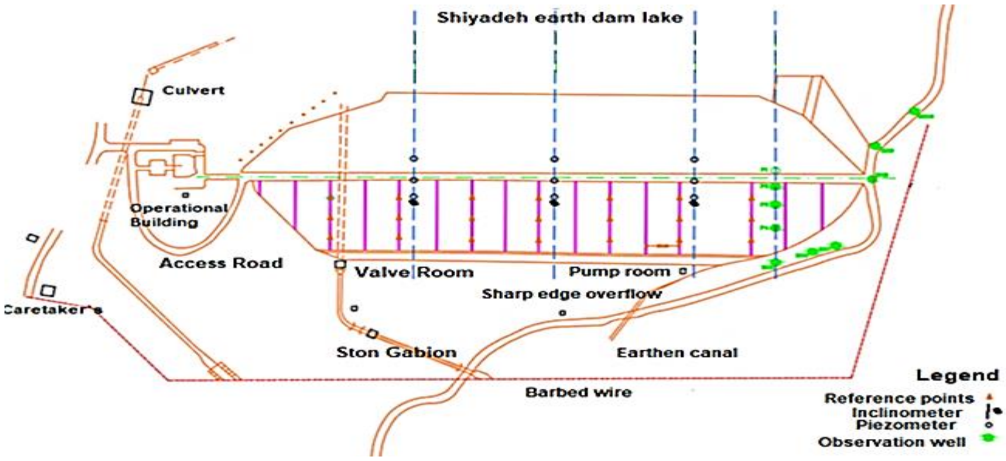

Fig. 18: The layout plan of the instrumentation and observation well of the dam

Initially, the settlement prediction for instrumentation C5 at level 189.84 was carried out using 530 recorded data entries in MATLAB R2019a software, and after analysis, In Figure 22, the prediction of settlement data using the RBF neural network is shown, highlighted in red.

From 1999 to 2012, all geotechnical instrumentation installed in the dam functioned properly, with no faults or malfunctions reported. During this period, settlement values were accurately recorded and are displayed in blue in Figure22.

To predict the settlement for the year 2024, a customized program was developed in MATLAB to simulate and reproduce the settlement trend by considering the historical pattern from 1999 to 2012. As a result of this modeling process, the predicted settlement for 2024 was obtained and is shown in red in Figure 19.

Enter the Error value and Error Spread constant, and after running the code, the network begins training to fit the existing data. With the completion of the training process, as shown in Figures 20, it can reach the desired error level.

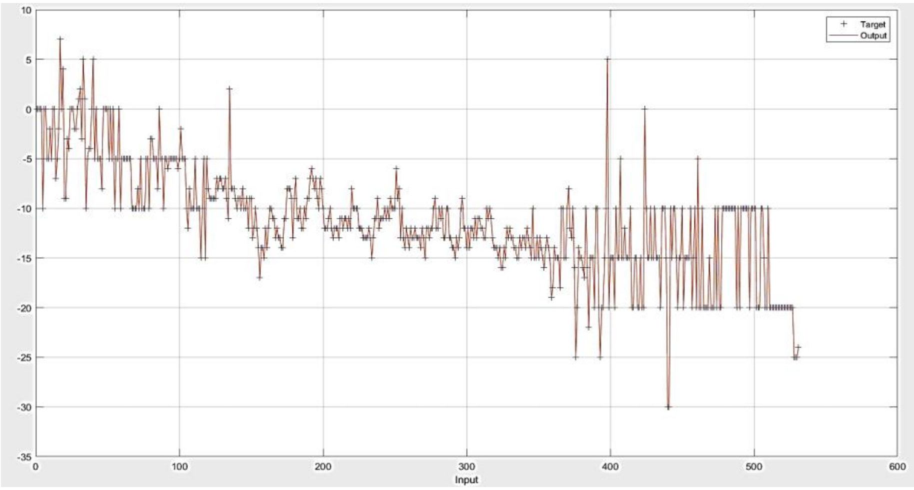

Fig. 19: Prediction of settlement data with the RBF neural network in red

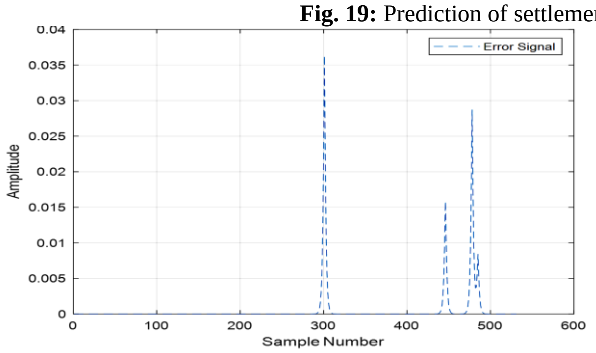

Fig. 20: Error Function

The results from the neural network system (Figure 21) indicate a predicted value of -24 mm, denoted by an asterisk (*).

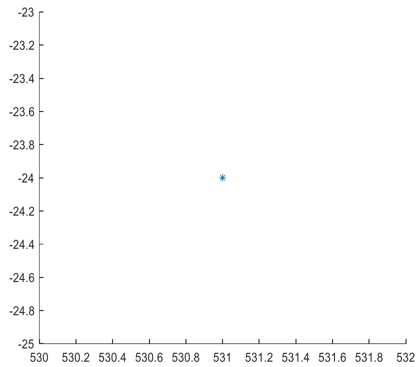

Fig. 21: Prediction results from the neural network system

In Table 3, the results of the predicted settlement values (in millimeters) using the neural network are presented for the instrumentation installed at cross-sections A-A, B-B, and C-C on the downstream slope, located at distances of 120, 220, and 318.52 meters from the left abutment of the dam.

Table 3: Predicted settlement results of instrumentation using the RBF neural network

Elevation code of the installed instrumentation	Prediction of settlement value using the neural network (mm)
A1 (179.60)	10
A2 (180.11)	-13
A3 (182.75)	-18
A4 (186.42)	-19
A5 (190.19)	-15
A6 (193.98)	-5
B1 (178. 0)	8
B2 (178.51)	-8
B3 (181.27)	-18
B4 (185.04)	-37
B5 (188.83)	-35
B6 (196.33)	-2
C1 (176.24)	15
C2 (178.9)	-8
C3 (182.53)	-27
C4 (186.19)	-31
C5 (189.84)	-24

In this study, the performance of two machine learning models—Radial Basis Function (RBF) neural network and Support Vector Machine (SVM) with RBF kernel—was compared on a specific dataset. The results indicate that the RBF network achieved superior accuracy, with a Root Mean Square Error (RMSE) of 0.0100, Mean Absolute Error (MAE) of 0.0025, and a coefficient of determination (R2)=1.0000, indicating an almost perfect fit to the target data. In contrast, the SVM model yielded an RMSE of 2.2612, MAE of 1.3287, and R2=0.9289, demonstrating comparatively lower predictive accuracy as shown in Table 4.

Table 4: Comparision of RFB and SVM

Performance Metric	RBF Network	SVM (RBF Kernel)
Root Mean Square Error (RMSE)	0.01	2.261
Mean Absolute Error (MAE)	0.0025	1.3287
Cofficient of Determination (R^2)	1.0	0.9289

This significant performance gap can be attributed to several factors. Primarily, the nature of the dataset appears to be smooth, continuous, and characterized by very low noise. The RBF network, utilizing radial basis functions, is inherently well-suited for approximating smooth and continuous functions, enabling it to closely model the underlying data patterns with minimal error.

On the other hand, the SVM with RBF kernel relies heavily on proper tuning of hyperparameters such as the regularization parameter CCC and the kernel width parameter γ\gammaγ. Without rigorous hyperparameter optimization, the SVM's ability to generalize accurately is compromised, likely explaining the observed performance drop. Moreover, SVMs typically exhibit better robustness in noisy data scenarios or when decision boundaries are complex; however, in this case, where the data structure is relatively simple and smooth, the RBF network's approximation capability proves more effective.

Furthermore, dataset size and dimensionality also play a crucial role in model selection. The RBF network's relatively simple architecture and faster training time make it particularly suitable for small to medium-sized datasets with low-dimensional input features. Conversely, SVMs, although computationally more intensive, can provide better generalization in large-scale and high-dimensional problems, provided that hyperparameters are carefully optimized.

In conclusion, these findings highlight the importance of considering data characteristics and model tuning when selecting an appropriate learning algorithm. The RBF network, due to its simplicity and high accuracy in approximating smooth, low-noise data, emerged as the preferred model for the present task. However, for more complex and noisy datasets, thorough hyperparameter optimization of SVMs may yield superior performance.

8. NUMERICAL INVESTIGATION

This study involved performing a three-dimensional static and dynamic analysis using PLAXIS software, considering the entire dam structure, foundation, and the interaction between the foundation and the embankment dam body. In Figure 22, the effective width required for the three-dimensional calculations is specified. To determine the optimal effective width of a homogeneous earth dam in terms of height PSO, CUCKOO, and IWO algorithms were used in two-dimensional analysis with PLAXIS software. All methods reached the same result, B = 1.81H. Therefore, in this study, the optimal effective width was considered based on the dam's height [46-49].

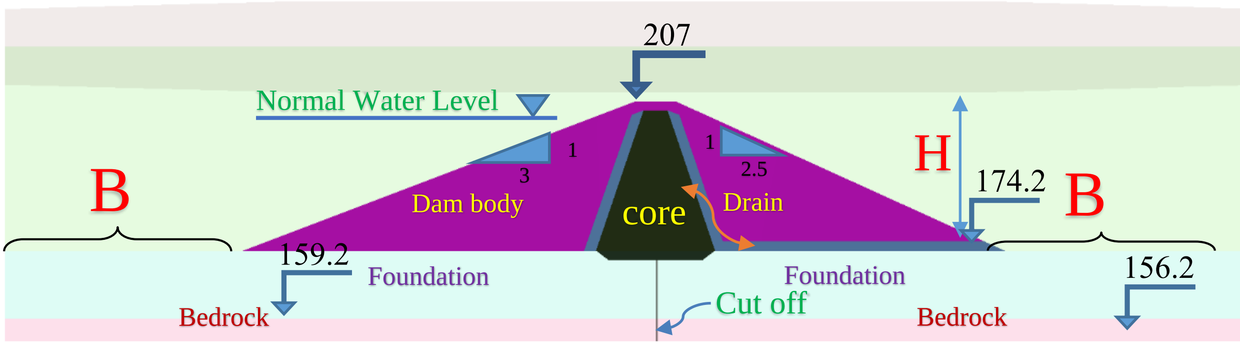

Fig. 22: The effective width in the 3D model of an earth dam

In this study, the acceleration-time record of the Manjil earthquake was used for the dynamic analysis of the Shiadeh earth dam. One of the earthquakes that caused significant destructive effects in the Alborz region was the Manjil earthquake, which occurred in 1990 at the Abbar station. This earthquake recorded a peak ground acceleration (PGA) of 0.51g, a peak ground velocity (PGV) of 0.43 m/s, and a peak ground displacement (PGD) of 0.18 m. The magnitude of this event was Mb=7.3 and Ms=7.7, indicating the release of a considerable amount of seismic energy. In the seismic design of the Shiadeh earth dam, and based on an intended service life of 75 years, a design basis earthquake (DBE) with a moment magnitude (Mw) of 7.1 has been considered. Through the integration of results obtained from probabilistic seismic hazard analysis (PSHA), the expected ground motion parameters at the dam site have been estimated as follows: Peak Ground Acceleration (PGA) = 0.37g, Peak Ground Velocity (PGV) = 0.34 m/s and Peak Ground Displacement (PGD) = 0.16 m. By comparing these values with those of the Manjil earthquake, it is evident that all corresponding parameters for the Shiadeh dam design earthquake are lower. This indicates that the current design includes a reasonable safety margin, ensuring the dam’s stability under potential future seismic events of similar or lower intensity.

To evaluate the interaction effects among the foundation, dam body, reservoir, and lateral supports as a single integrated system, the Manjil earthquake record was used for modeling in PLAXIS software (Figure 23). It should be noted that PLAXIS software is considered a reliable and suitable tool for solving dynamic analysis problems in modeling the dam body, foundation, and reservoir.

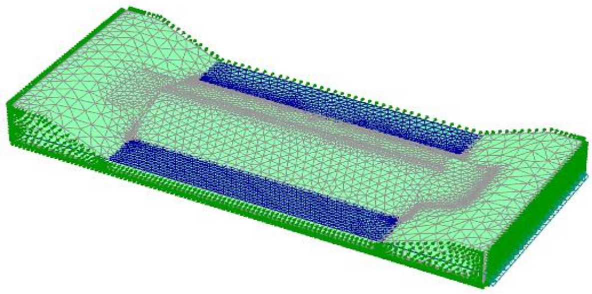

Fig. 23: The components of the body, supports, and the effective width

To determine the settlement and monitor the earth dam at the locations where the instrumentation has been installed, existing recorded data from the instrumentation over the years when they were functioning properly should be utilized. Subsequently, for trend analysis, by writing a program in MATLAB and using the powerful RBF algorithm, it will be possible to obtain the settlement values at the designated points.

To account for the effect of a secondary fault in the three-dimensional PLAXIS model, it is essential to conservatively modify the mechanical properties of the soil mass in the faulted zone. Accordingly, parameters such as cohesion, internal friction angle, and elastic modulus are reduced, while the permeability is increased to realistically simulate potential instability and slip.

These modifications have been specifically applied to the left abutment of the dam site, where geological evidence indicates the presence of a secondary fault and the likely degradation of geotechnical properties.

Table 5 presents the specifications of the earth dam, which were prepared by the geotechnical consultant and approved by Khazar Ab Consulting in 1998. These specifications were used as the parameters of the dam's various components in the three-dimensional PLAXIS model.

These parameters typically include the engineering and behavioral characteristics of different geological layers, materials, and various structural sections of the dam, such as the core, filter, shell, and other components [50].

TABLE 5. Characteristics of homogeneous Shiadeh Dam earth materials

Parameter	Type	core	Filter	Shell	Left support layer	Right support Gravel	Riverbed Gravel	Impermeable layer	Cutoff & Retaining wall	Unit
Behavioral Model	Model	Soft Soil	Hardening Soil	Hardening Soil	Soft Soil	Hardening Soil	Hardening Soil	Non porous	Liner Elastic	-
Type of Drainage	-	undrained	drained	drained	undrained	drained	drained	undrained	undrained	-
Specific weight above the water table	γ_{unsat}	18.8	18	21.8	17	21	21.2	22	25	KN/m^3
Specific weight at groundwater table	γ_{sat}	19.8	20	22.2	19	21	22	22	25	KN/m^3
Young's Modulus	E	-	60E3	60E3	-	60E3	54E3	5000	23.5e6	KN/m^2
Shear Modulus	G	-	-	-	-	-	-	2174	10.22e6	KN/m^2
Poisson' Ratio	ν	0.2	0.2	0.2	0.15	0.2	0.2	0.15	0.15	-
Adhesion	C	50	2	2	16	10	2	150	-	KN/m^2
Internal Friction angle	Ø	19	30	35	17	24	34	25	-	-
Angle of Dilation	Ψ	0	0	5	0	0	4	0	-	-
Incremental Young's Modulus	E_{ur}	-	180E3	180E3	-	180E3	162E3	-	-	KN/m^2
Permeability Coefficient	K_x,k_y	0.864E-3	0.864	0.864	0.864E-3	0.0864	0.864	1E-6		m/day
λ^*	-	0.106	-	-	0.106	-	-	-	-	-
κ^*	-	0.055	-	-	0.055	-	-	-	-	-

9. DYNAMIC ANALYSIS

One of the earthquakes with significant destructive effects in the Alborz region was the Manjil earthquake, which occurred in June 1990. Its magnitude was Mb=7.3 and Ms=7.7. The settlement of the earth dam was determined using 3D PLAXIS software across 13 phases:

1. Initial phase: The current state of the riverbed and the left and right abutments of the dam.
2. Phase 1: Excavation of the trench, construction of the retaining wall, and implementation of a cutoff to the foundation depth.
3. Phase 2: Construction of the earth dam.
4. Phase 3: Reservoir filling up to the maximum level (normal level).
5. Phase 4: Safety factor for a full reservoir.
6. Phase 5: Rapid drainage of the reservoir.
7. Phase 6: Safety factor for rapid drainage of the reservoir.
8. Phase 7: Slow drainage of the reservoir.
9. Phase 8: Safety factor for slow drainage of the reservoir.
10. Phase 9: Represents the reservoir's minimum water level.
11. Phase 10: Denotes the safety factor for the reservoir's minimum water level.
12. Phase 11: Application of an earthquake to the earth dam after the construction is completed.
13. Phase 12: Application of an earthquake to the earth dam with a full reservoir up to the normal level.

Figure 24 shows the maximum acceleration of 0.28 g related to the normalized acceleration time history of the Manjil earthquake with the SEISMOSIGNAL 2022 software, which is considered under the maximum design level (MDL) and used in the modeling.

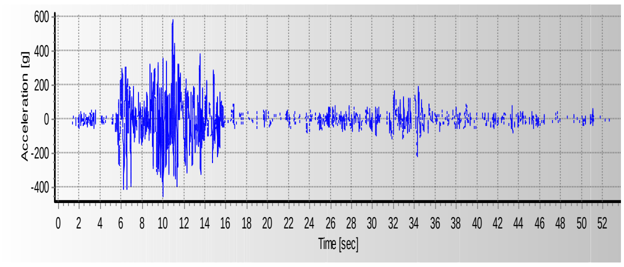

Fig. 24: Acceleration mapping of the first component of the Manjil earthquake with SEISMO SIGNAL 2022 software

Since the concrete structure in contact with the soil has experienced a 0.67 reduction in strength, it is necessary to define interfaces for the entire contact surface between the concrete retaining wall and the soil, as well as in the impervious Cut-Off layer. Interfaces must also be considered for the side supports.The boundary condition coordinates, shown in red, are defined separately in Figure 25 as follows:

The settlement results, or maximum vertical deformation under dynamic loading along the dam crest, are presented in two scenarios:

At the groundwater level upstream in the xz plane: {(0,0,0), (-20,0,0), (0,0,450), (-20,0,450)}

At the river level in the xy plane: {(0,0,0), (0,0,430), (0,-60,0), (0,-60,430)}

At the maximum reservoir level on the upstream slope: {(0,0,0), (33,99,-10), (33,99,440), (0,0,430)}

Maximum Settlement: As depicted in Figure 26, the maximum settlement along the dam crest, when the reservoir is filled to its normal level, is 0.789 meters. The maximum settlement in Figure 27, along the dam crest in the post-construction state, is 0.698 meters.

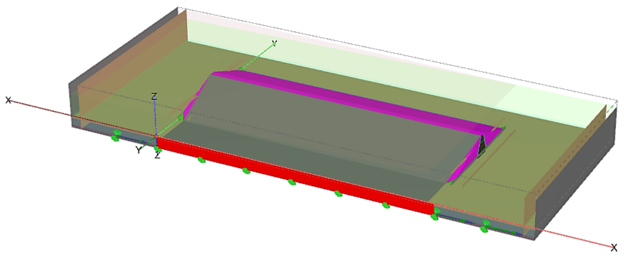

a) Groundwater level at upstream in xz plane

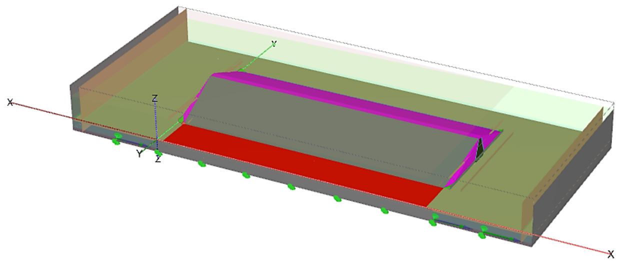

b) River level in xy plane

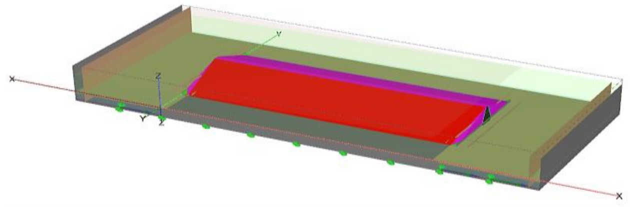

c) Maximum reservoir level on upstream slope

Fig. 25: Boundary condition coordinate points

In the 3D numerical model, the reservoir impoundment process was simulated in 13 sequential phases, during which all relevant settlement conditions were evaluated. The maximum recorded deformation along the crest was 78.09 mm. Given that the Shiadeh earth dam is classified as a vital and high-importance structure in the region, the development of an Early Warning Protocol (EWP) is essential—even in cases where only limited data and information are available.

Establishing such a protocol requires the application of engineering knowledge to assess the dam's stability during its operational phase. To prevent potential human and financial losses, the formulation of this protocol necessitates collaboration among experts in various fields such as geotechnical engineering, surveying, geology, and other related disciplines. In this context, PLAXIS software has been employed as a reliable and effective tool for both static and dynamic analysis, allowing for integrated modeling of the dam body, foundation, and reservoir. The settlement behavior of the Shiadeh earth dam was modeled and evaluated using the 3D version of PLAXIS software across 13 distinct phases, corresponding to various reservoir water levels during different seasons of the year, with a high level of precision.

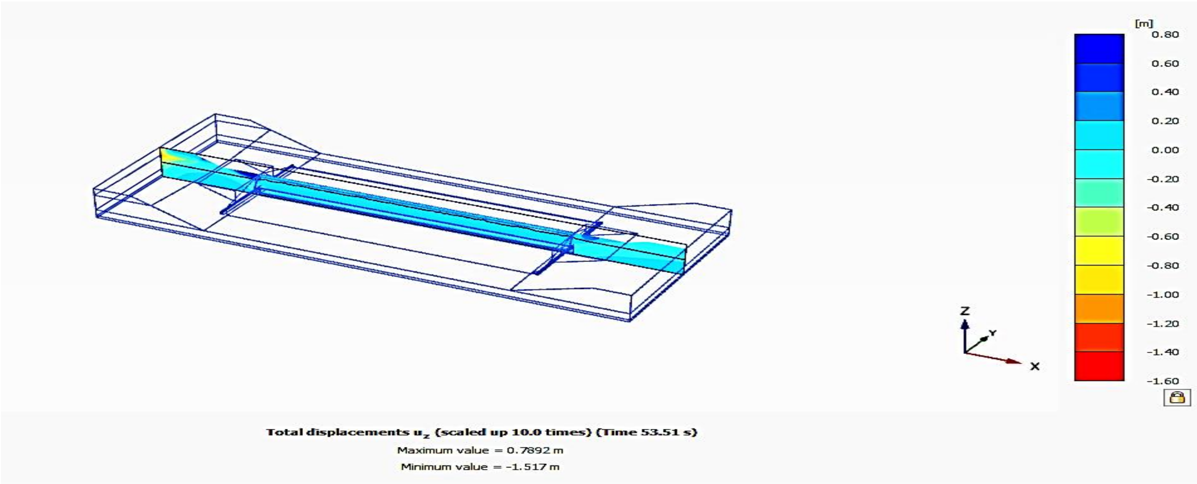

Fig. 26: The settlement along the dam crest in the case of a full reservoir

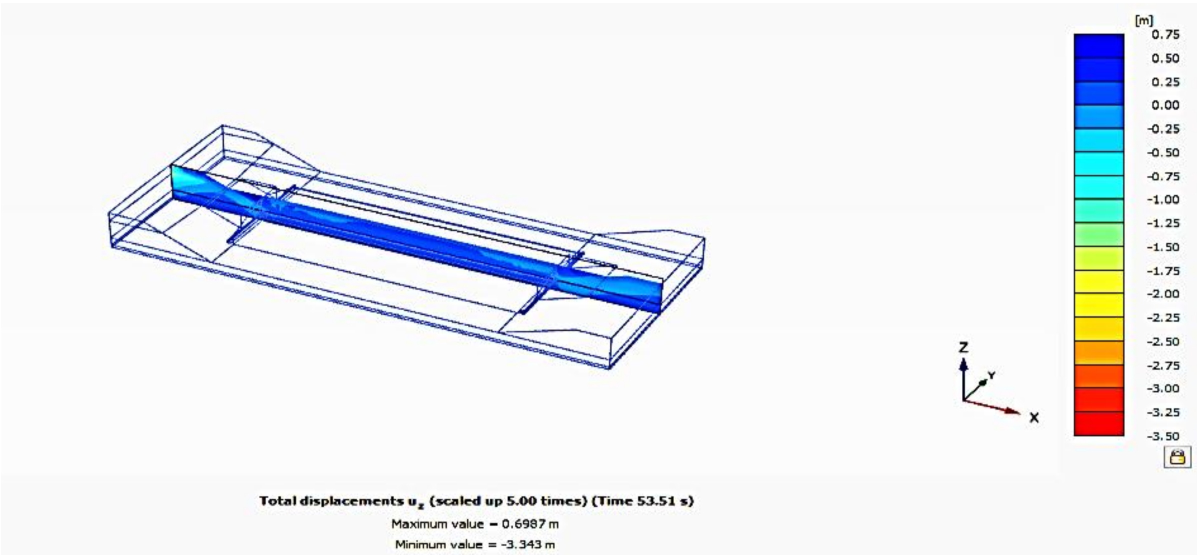

Fig. 27: The settlement along the dam crest in the post-construction

Establishing such a protocol requires the application of engineering knowledge to assess the dam's stability during its operational phase. To prevent potential human and financial losses, the formulation of this protocol necessitates collaboration among experts in various fields such as geotechnical engineering, surveying, geology, and other related disciplines. In this context, PLAXIS software has been employed as a reliable and effective tool for both static and dynamic analysis, allowing for integrated modeling of the dam body, foundation, and reservoir. The settlement behavior of the Shiadeh earth dam was modeled and evaluated using the 3D version of PLAXIS software across 13 distinct phases, corresponding to various reservoir water levels during different seasons of the year, with a high level of precision.

Settlement analysis results along the crest of the dam were examined for all 13 phases, and the two scenarios of maximum vertical settlement or deformation are presented in Figures 25 and 26. Additionally, in the 13-phase analysis, the factor of safety obtained from the 3D PLAXIS model ranges between 1.00 and 1.15, which is in full compliance with the standards outlined in Publication No. 624: Guidelines for Seismic Analysis and Design of Earth and Rockfill Dams.

10. DISCUSSION

In this study, a predictive model for downstream slope and dam crest failure is developed using a preventive approach. This model is based on neural networks and an analysis of integrated numerical data obtained from field instruments and the Finite Element Method (FEM). The cornerstone of the slope failure prediction process is the creation of a robust model utilizing field instrument data and numerical analysis. It is crucial to acknowledge that various factors affect this prediction model, including precipitation, inadequate surface and subsurface drainage, slope surface erosion due to alternating dry and wet cycles, and inappropriate soil types. Climate change scenarios emphasizing increased precipitation and intensified wet and dry cycles have been highlighted by many researchers. In this study, the climatic conditions of the dam site region were considered as an influential factor; however, the direct impact of these changes has not been examined within the early warning protocol. Therefore, a more comprehensive assessment and analysis of climate change effects on dam performance and safety is recommended in future studies to provide a better response to potential environmental variations.

This research seeks to establish a comprehensive framework for designing a strong quantitative and qualitative predictive model. Considering all the influencing variables in the construction of the EWP protocol for slope failure, this research framework is crucial for final decision-making. The practical research framework for the Early Warning Protocol (EWP) for earth dam slopes consists of four key sections: observation, planning, decision-making, and action. For successful implementation of an Early Warning System (EWS) for slope failures, the subcomponents of this framework must be executed effectively. The Early Warning Protocol includes several stages. In the observation stage, vulnerable slopes are identified and listed, and the impact of failure-causing factors is determined. In the planning stage, existing monitoring methods are identified, and initial prediction models are designed. In the decision-making stage, monitoring and stabilization methods are evaluated in terms of cost-effectiveness. Finally, in the action stage, critical slopes in dams are prioritized, and action programs are evaluated and implemented.

11. CONCLUSION

Early warning protocols are essential for safeguarding the safety and integrity of infrastructure. A well-structured early warning system can effectively detect potential risks and provide adequate time for corrective actions to be implemented. Such a system follows a systematic process of identifying risks, monitoring and analyzing data, and issuing warnings to relevant stakeholders. Advancements in technologies, such as sensors and satellite imagery, have enabled more efficient and accurate data collection and analysis.

For an early warning protocol to be successful, cooperation among various stakeholders, including engineers, researchers, and government agencies, is crucial. By establishing a robust and efficient early warning system, potential risks to infrastructure can be identified and mitigated, ensuring public safety and well-being. The development of an early warning protocol offers numerous advantages: it enables the timely detection of potential hazards, gives decision-makers sufficient time to take corrective actions to minimize risks, reduces the likelihood of infrastructure damage, ensures public safety by providing enough time for evacuation or other protective measures, decreases the risk of disruptions in essential services and supply chains, supports the uninterrupted functioning of critical services, improves resource planning and management, and helps build public confidence in infrastructure by demonstrating a commitment to safety and preparedness.

The Shiadeh Earth Dam was first impounded in 1999. A comparison of the dam's settlement from 1999 to 2012, measured at a distance of 118.4 meters from the left abutment, revealed the highest recorded settlement during this period. However, satellite imagery could not be used for settlement analysis until 2014. By preprocessing satellite data using the SNAP software, the settlement between 2014 and 2024 was determined to be 87 centimeters. Additionally, a 3D analysis conducted using PLAXIS software, considering all impoundment phases and static and dynamic loading conditions with an appropriate safety factor, estimated a total settlement of 78.09 centimeters, which aligns well with the results obtained from satellite image processing. The discrepancy in settlement between the satellite imagery and the 3D PLAXIS analysis can be attributed to the presence of a secondary fault at the left abutment. The calibration process was independently carried out for both the PLAXIS and InSAR methods.

In the three-dimensional numerical modeling using PLAXIS software, all geotechnical parameters including elastic modulus, cohesion, internal friction angle, and permeability were directly obtained from Table 4, which summarizes the results of field and laboratory tests conducted on eight boreholes. Since these parameters were selected based on comprehensive and well-documented geotechnical data, conducting a sensitivity analysis for the soil properties was deemed unnecessary. For the InSAR method, calibration was performed according to a standard procedure. As shown in Figure 8, all necessary corrections including satellite system errors, topographic influences, and atmospheric disturbances were carefully applied. These corrections ensured that the measured surface displacements accurately reflected the actual ground deformations along the crest of the earth dam. The impact of secondary fault on the left abutment has caused downstream sliding at the left abutment and toe sliding in areas adjacent to the left abutment. After the occurrence of surface sliding at the toe of the downstream slope and slipping in the lower left bank abutment, the Mazandaran Regional Water Company promptly undertook stabilization and repair of the damaged sections. At present, no visible signs of landslides or instability have been observed or reported in the vicinity of the Shiadeh dam. However, due to the dam site's proximity to active faults, as well as the presence of a secondary fault in the region, the potential for future slope movement cannot be ruled out. Accordingly, the stability status of the Shiadeh dam has been assessed at Alert Level 2 (Precautionary Stage). In other words, it is essential to implement continuous monitoring measures—particularly through non-structural methods such as satellite image analysis and precise ground-based surveying along the dam crest and micro-geodetic stations—on a periodic basis. These actions are necessary to detect and control any potential deformations or displacements at the earliest possible stage. In this study, several comprehensive steps were taken to validate and ensure the reliability of the proposed protocol. Based on the analysis results, a structured observation and timely action plan was identified as the core component of the protocol. The integration of modern technologies within a cohesive framework offers a new perspective for monitoring earth dams and managing associated risks. By combining extensive satellite monitoring capabilities, the accuracy of numerical modeling, the predictive power of advanced algorithms, and field validation, a comprehensive and reliable early warning system can be designed—one that serves as an effective step toward enhancing the safety of the country's water infrastructure. This protocol presents an innovative, scientific, and practical approach for monitoring the Shiadeh earth dam under specific conditions and with minimal available data, leveraging the advantages of state-of-the-art technologies. Implementation of this system enables early detection of abnormal behaviors, crisis prediction, and reduction of potential damages caused by dam failures.

It is recommended that this category of dams be entrusted to a multidisciplinary research team (including geotechnics, geology, crisis management, economics, and programming). Therefore, completing geological and geotechnical studies is essential to determine the slope of the foundation soil layers and fault fractures to assess potential water leakage from the reservoir. Additionally, the destructive impact of secondary faults from a geological perspective must be thoroughly investigated.

References

[1] Nobahar M, Khan MS, Alzeghoul OE, Graham G, Young K. Condition Assessment of a HWS Using Field Instrumentation and Electrical Resistivity Imaging (ERI). In Geo-Congress 2022, pp. 102-112.

[2] Nobahar M, Khan MS, Ivoke J. Combined effect of rainfall and shear strength on the stability of highway embankments made of Yazoo clay in Mississippi. Geotechnical and Geological Engineering, 2020, 38(3), 2787-2802.

[3] Nobahar M, Khan MS, Salunke R, Gardner A, Chia KH. Moisture Variation Monitoring of Failed and Not-Failed Highway Slope through Resistivity Imaging in Mississippi. In Geo Congress 2022, pp. 72-81.

[4] Nobahar M, Salunke R, Alzeghoul OE, Khan MS, Amini F. Mapping of Slope Failures on Highway Embankments using Electrical Resistivity Imaging (ERI), Unmanned Aerial Vehicle (UAV), and Finite Element Method (FEM) Numerical Modeling for Forensic Analysis, Transportation Geotechnics, Volume 40, 2023, 100949, ISSN 2214-3912.

[5] Nobahar M, Salunke R, Khan MS, Amini F. Development of Soil Moisture Content and Soil Matric Suction Model Based on Field Instrumentation and Electrical Resistivity Imaging (ERI) for Highway Slopes Constructed on High Expansive Clay Soil. Geotechnics, 2022, 2(3), 569 671-705.

[6] Nobahar M. An Early Warning Protocol Against Highway Slopes Failure On Expansive Soil." Jackson State University, Mississippi, USA, 2022.

[7] Khan MS, Amini F, Nobahar M. Performance Evaluation of Highway Slopes on Yazoo Clay. Mississippi. Dept. of Transportation, 2020.

[8] Ivoke John, Unsaturated Hydraulic Conductivity Variation of Expansive Yazoo Clay with Wet- Dry Cycles. (2021) https://doi.org/10.1177/03611981211011994

[9] Kandalai S, John NJ, Patel A. Effects of Climate Change on Geotechnical Infrastructures— state of the art. Environmental Science and Pollution Research, 2023 Jan 5:1-27.

[10] Vahedifard F, Adaptation strategies for levees under a changing climate.2022

[11] Bračko T, Žlender B, Jelušič P. Implementation of Climate Change Effects on Slop Stability Analysis. Applied Sciences. 2022 Aug 16;12(16):8171.

[12] Allard RF. Climate change adaptation: Infrastructure and extreme weather. Industry, Innovation, and Infrastructure. 2021:105-16.500

[13] Fant C, Jacobs JM, Chinowsky P, Sweet W, Weiss N, Sias JE, Martinich J, Neumann JE. Mere nuisance or growing threat? The physical and economic impact of high tide flooding on US road networks. Journal of infrastructure systems. 2021 Dec 1;27(4):04021044.

[14] Karagiannis GM, Cardarilli M, Turksezer ZI, Spinoni J, Mentaschi L, Feyen L, Krausmann E. Climate change and critical infrastructure–storms. European Union: Luxembourg. 2019

[15] Pk S, Bashir R, Beddoe R. Effect of climate change on earthen embankments in Southern Ontario, Canada. Environmental Geotechnics. 2018 Dec 18;8(2):148-69.

[16] Xu Y, Su C, Huang Z, Yang C, Yang Y. Research on the protection of expansive soil slopes under heavy rainfall by anchor-reinforced vegetation systems. Geotextiles and Geomembranes. 2022 Dec 1;50(6):1147-58.

[17] Liang C, Wu Z, Liu X, Xiong Z, Li T. Analysis of shallow landslide mechanism of expansive soil slope under rainfall: a case study. Arabian Journal of Geosciences. 2021 Apr;14:1- 531 1.

[18] Nobahar M, Khan MS, Ivoke J, Amini F. Impact of rainfall variation on slope made of expansive Yazoo clay soil in Mississippi." Transportation Infrastructure Geotechnology, 2019, 6(4), 318-336.

[19] Nobahar M, Khan MS. Prediction of Matric Suction of Highway Slopes Using Autoregression Artificial Neural Network (ANN) Model. In Geo-Extreme 2021, pp. 40-50.

[20] Khan MS, Ivoke J, Nobahar M, Amini F. Artificial Neural Network (ANN) based Soil Temperature model of Highly Plastic Clay. Geomechanics and Geoengineering, 2022, 17(4), 1230-1246

[21] Abrams TG, Wright SG. A survey of earth slope failures and remedial measures in Texas.4971972 Dec

[22] Wright SG. Evaluation of soil shear strengths for slope and retaining wall stability analyses with emphasis on high plasticity clays. Project No. 5-1874. 2005 Aug;1.

[23] Lee Jr LT. State Study 151 and 236: Yazoo Clay Investigation, 2012, No. FHWA/MS- DOT-RD-11-236.

[24] Nelson J, Miller DJ. Expansive soils: problems and practice in foundation and pavement engineering. John Wiley & Sons, 1997.

[25] Kongai F, Impact of Pit latrines on Groundwater Quality: A comparative study of boreholes and protected springs in Mpigi Town Council, Uganda,2023

[26] Wanare R, Iyer KK, Jayanthi P. Recent advances in early warning systems for landslide forecasting. Geohazard Mitigation: Select Proceedings of VCDRR 2021. 2022:249-60.

[27] Fawzy S, Strategies for mitigation of climate change: a review.2020

[28] Petley D. Global patterns of loss of life from landslides. 2012

[29] Tavakoli MA,Fathipour H, Payan M. Seismic bearing capacity of shallow foundations subjected to inclined and eccentric loading using modified pseudo-dynamic method. Transportation Geotechnics. Volume 40, May 2023, 100979.

[30] Fathipour H, Siahmarzgi AH, Payan M. Evaluation of the active and passive pseudo-dynamic earth pressures using finite element limit analysis and second-order cone programming.Volume 41, pages 1921–1936, (2023).

[31] Fathipour H, Javankhoshdel S, Payan M. Probabilistic Assessment of Seismic Bearing Capacity of Strip Footings Seated on Heterogeneous Slopes Using Finite Element Limit Analysis (FELA) and Response Surface Method (RSM). TMIC 2022, AHE 13, pp. 199–209, 2023.

[32] Payan M , Asadi p, Jamaldar AH. Artificial intelligence-based predictive models for shear wave velocity of soils: A comprehensive review. Accepted 5 May 2025.

[33] Fatehi M, Hosseinpour I, Payan M .Deterministic Seismic Stability Analysis of Reinforced Slopes using Pseudo-Static Approach. Iranian Journal of Science and Technology, Transactions of Civil Engineering. Accepted: 3 September 2022

[34] Kjekstad O, Highland L. Economic and social impacts of landslides. In Landslides–disaster risk reduction. Springer, Berlin, Heidelberg, 2009, pp. 573-587.

[35] The Mazandaran Regional Water Company Control and Stability Report, (1999-2024)

[36] G. E. Fasshauer, Meshfree Approximation Methods with MATLAB, Vol. 6, World Scientific Publishing Co., Inc., River Edge, NJ, USA, 2007.

[37] Massonnet, D., Feigl, K.L. (1998). Radar interferometry and its application to changes in the Earth's surface. Reviews of Geophysics, 36(4): 441-500. https://doi.org/10.1029/97RG03139

[38] Simons, M., Rosen, P.A. (2007). Interferometric synthetic aperture radar geodesy. Geodesy, 3: 391-446. https://doi.org/10.1016/B978-044452748-6.00059-6

[39] Goudarzi, M. A.: Detection and measurement of land deformations caused by seismic events using InSAR, Sub-pixel correlation, and Inversion techniques, p. 7, https://webapps.itc.utwente.nl/librarywww/papers_2010/msc/gem/goudarzi.pdf, (last access: 8 May 2022), 2010.

[40] Kim, J. W.: Applications of Synthetic Aperture Radar (SAR)/SAR Interferometry (InSAR) for Monitoring of Wetland Water Level and Land Subsidence, Ohio State Univ., 1–111, https://core. ac.uk/download/pdf/159596183.pdf (last access: 8 May 2022), 2013.

[41] Netzband, M., Stefanov, W. L., and Redman, C.: Applied remote sensing for urban planning, governance and sustainability, Springer, https://doi.org/10.1007/978-3-540-68009-3, 2007.

[42] Mondini, A.C., Santangelo, M., Rocchetti, M., Rossetto, E., Manconi, A., Monserrat, O. (2019) Sentinel-1 SAR amplitude imagery for rapid landslide detection. Remote Sensing, 11(7): 760. https://doi.org/10.3390/rs11070760

[43] Ommati, M. (2022). FaraDars. www.Faradars.org

[44] The Mazandaran Regional Water Company Control and Stability Report, (1999-2024)

[45] Report of the Shiadeh Dam Project, Regional Water Company of Mazandaran Province, (1998).

[46] Anisheh, S. R. Sarifipour. M. Optimization of the effective width of the foundation of a homogeneous earth dam under earthquake using the IWO algorithm. Internatıonal Journal of Natural and Engineering Sciences E-ISSN: 2146-0086 18 (2): 77-91, 2024.

[47] Anisheh, S. R. Anisheh S. M. Application of Finite Difference Method and PSO Algorithm in Seismic Analysis of Narmab Earth Dam. International Journal of Computer Applications (0975 – 8887) Volume 54– No.1, September 2012.

[48] Anisheh, S. R., Anisheh, S. A., & Anisheh, S. H. Seismic analysis of Narmab earth dam and optimization of its parameters using cuckoo. Internatıonal Journal of Natural and Engineering Sciences. E-ISSN: 2146-0086 13 (2): 53-58, 2019

[49] Farrokhi, F., Rasouli, R., Anisheh, S.R . Seismic Analysis of Homogeneous Earth Dam and Optimization of Its Parameters Using Pso. Internatıonal Journal of Natural and Engineering Sciences E-ISSN: 2146-0086 12 (1): 42-48, 2018.

[50] Report of the Shiadeh Dam Project, Khazar Ab Consulting in 1998.